CHALMERS

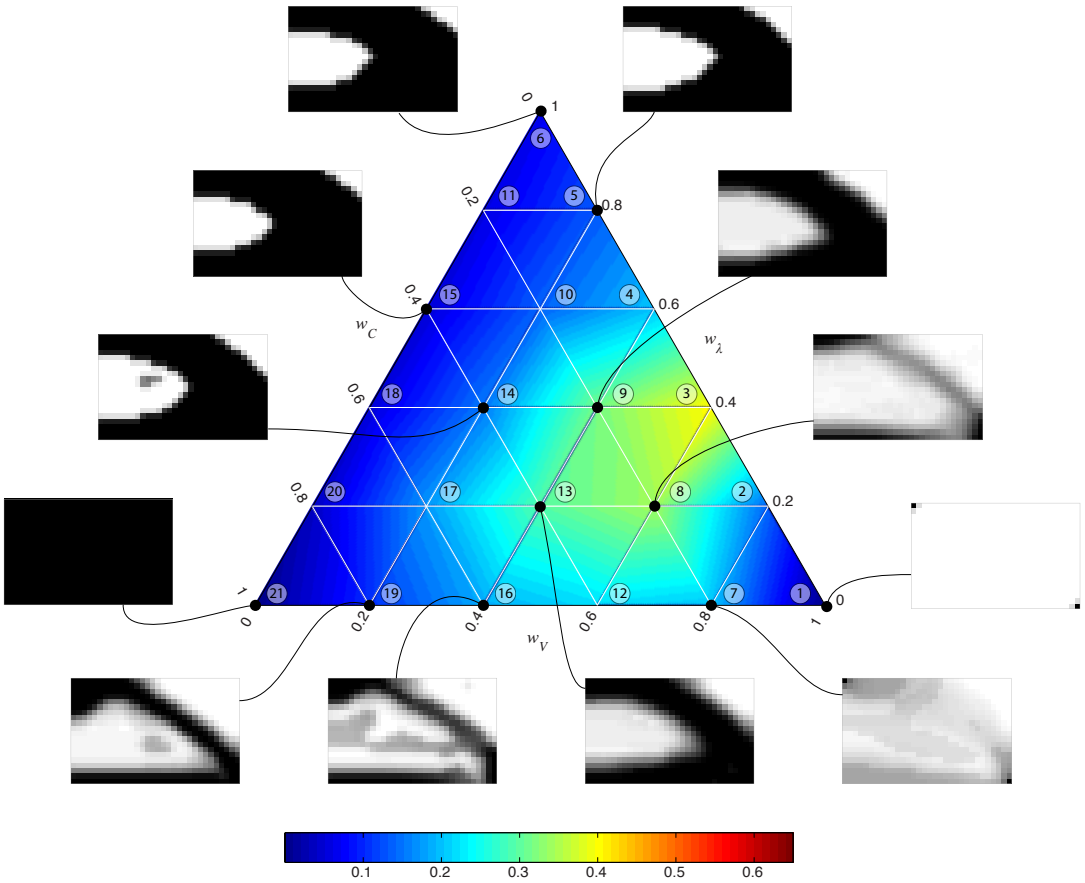

Multi-Objective Topology Optimization

Tracing of Pareto-optimal structures with respect to volume, compliance and fundamental eigenvalue

Master's thesis in Structural Engineering and Building Technology

ALEXANDER SEHLSTRÖM

Department of Applied Mechanics
Division of Dynamics and *Division of Material and Computational Mechanics*
CHALMERS UNIVERSITY OF TECHNOLOGY
Gothenburg, Sweden 2013
Master's thesis 2013:18

MASTER'S THESIS IN STRUCTURAL ENGINEERING AND BUILDING TECHNOLOGY

Multi-Objective Topology Optimization

Tracing of Pareto-optimal structures with respect to volume, compliance and fundamental eigenvalue

ALEXANDER SEHLSTRÖM

Department of Applied Mechanics
Division of Dynamics and *Division of Material and Computational Mechanics*
CHALMERS UNIVERSITY OF TECHNOLOGY

Gothenburg, Sweden 2013

Multi-Objective Topology Optimization
Tracing of Pareto-optimal structures with respect to volume, compliance and fundamental eigenvalue
ALEXANDER SEHLSTRÖM

Master's thesis 2013:18
ISSN 1652-8557
Department of Applied Mechanics
Division of Dynamics *and* Division of Material and Computational Mechanics
Chalmers University of Technology
SE-412 96 Gothenburg
Sweden
Telephone: +46 (0)31-772 1000

Cover:
Compromise value and Pareto-optimal solutions for half of an MBB-beam optimized with respect to volume, compliance and fundamental eigenvalue.

Chalmers Reproservice
Gothenburg, Sweden 2013

Multi-Objective Topology Optimization
Tracing of Pareto-optimal structures with respect to volume, compliance and fundamental eigenvalue
Master's thesis in Structural Engineering and Building Technology
ALEXANDER SEHLSTRÖM
Department of Applied Mechanics
Division of Dynamics *and* Division of Material and Computational Mechanics
Chalmers University of Technology

ABSTRACT

Topology optimization, a subfield of structural optimization, is about finding the best connectivity between loads and supports with respect to some objectives. Topology optimization can e.g. be applied in order to find the shape of a beam or the reinforcement layout in a concrete slab. This thesis presents a formulation and solution approach for finding the Pareto-optimal solutions of multi-objective topology optimization problems. Objectives considered are the minimization of volume, the minimization of compliance under static loads, and the maximization of the fundamental eigenvalue of the structure under free vibration. The multi-objective formulation is done using compromise programming. It is found that the scaling parameters of this method have a large effect on the scope of the resulting Pareto-optimal solutions. The optimization problem is solved using a sequential linear programming (SLP) algorithm with interpolation schemes (ModSIMP and RAMP) to encourage integer solutions. Numerical instabilities are reduced using a mesh independent density filter along with a continuation method operating on the filter radius. The method has been implemented in Matlab and been used in order to solve the numerical examples presented in the thesis. Two numerical examples are considered: a simply supported beam and the support structure of a bridge deck. The obtained structures are comparable to the results of single objective topology optimization results based on the optimality criteria method, however the resulting structures are not as clear integer solutions as desired. Some possible reasons for this is discussed and a proposal for future work is presented.

Keywords: topology optimization, multi-objective optimization, structural engineering

Preface

This Master's Thesis comprises 30 credits and has been carried out during the spring of 2013. The work has taken place at Chalmers University of Technology (CTH) in Gothenburg, Sweden.

The project has been carried out under supervision of Dr Håkan Johansson, senior lecturer at CTH, Department of Applied Mechanics, Division of Dynamics, and Gennaro Senatore, EngD researcher at University College London and design systems analyst at Expedition Engineering, London, UK.

Dr Mats Ander, senior lecturer at CTH, Department of Applied Mechanics, Division of Material and Computational Mechanics, has acted as the examiner of this thesis.

Acknowledgements

First and foremost I want to thank my supervisors Dr Håkan Johansson and Gennaro Senatore for their continuous support; their help and encouragement has been most valuable and their different perspectives has strengthen the thesis. Examiner Dr Mats Ander also deserves a big thanks for his support and constant encouragement, especially when work has proceeded slowly and in unwanted directions.

I would also like to thank Dr Pete Winslow at Expedition Engineering for his help during the development of the scope of the thesis. Thanks are also due to Thomas Neidhart and Dr Mikio Braun, whom have contributed with support on the Apache Commons Math Java SIMPLEX solver and the jblas Java package, respectively, both key stone libraries in the Java application development.

At last I want to thank my fellow students Agnes Orstadius and Lukas Nordström for the discussions we have had during the project and for their feedback during the writing of the report.

Gothenburg, Sweden in June 2013

Alexander Sehlström

Nomenclature

Throughout this thesis, the following symbols apply. Symbols that are only used once are not listed below.

General

In general, the following symbols are used. The symbols may in some cases be overridden by chapter specific definitions.

Greek uppercase symbols

Ω	Design domain	
Ω_e	Element domain	
Ω^{fixed}	Part of design domain that is fixed (prescribed solid)	
Ω^{free}	Part of design domain that is free	
Ω^{mat}	Part of design domain that has material	
Ω^{passive}	Part of design domain that is passive (prescribed void)	

Greek lowercase symbols

λ	Eigenvalue	
λ_1	Lowest eigenvalue	
ν^0	Poisson's ratio, base material	
ρ_e	Generalized density, element e	[-]
$\tilde{\rho}_e$	Density filtered generalized density, element e	[-]
ρ_{min}	Generalized density, lower bound	[-]
ρ^0	Density, base material	[kg/m^3]

Greek bold lowercase symbols

$\boldsymbol{\rho}$	Vector of generalized densities	[-]
$\boldsymbol{\rho}^*$	Optimal generalized densities	[-]
$\boldsymbol{\rho}^0$	Vector of base material densities	[kg/m^3]

Roman italic uppercase symbols

C	Compliance	
E_e	Element Young's modulus	[Pa]
E_e^0	Element Young's modulus, base material	[Pa]
E_{min}	Young's modulus, minimum value	[Pa]
H_{ei}	Convolutionary weight factor for element e with respect to element i	

N_e	Element set for which the element centre-to-centre distance $\text{dist}(e, i)$ is smaller than the filter radius r_{min} where e is a predefined element and i is an arbitrary element	
V	Volume	[m^3]
V_Ω	Design domain volume	[m^3]
V_e	Element volume, elmenet e	[m^3]
V_e^0	Base volume, elmenet e	[m^3]

Roman italic lowercase symbols

f	Objective function	
f_V	Volume fraction	
$f_{V,\text{min}}$	Smallest reasonable volume fraction	
k	Weight point; the point has coordinates in weight factor space	
l_p	Compromise function	[-]
n_{el}	Number of elements	
n_f	Number of objective functions	
p	SIMP and ModSIMP penalization power (typically $p \geq 3$)	
p_n	p-norm order ($p_n \geq 1$)	
q	RAMP interpolation parameter	
r_{min}	Filter radius	[m]
t	Thickness	[m]
w_i	Weight factor for objective i	

Roman bold uppercase symbols

$\mathbf{K}$	Global stiffness matrix	[N/m]
$\mathbf{K}_e$	Element stiffness matrix, global coordinate system	[N/m]
$\mathbf{K}_e^0$	Element stiffness matrix, global coordinate system with unit Young's modulus ($E = 1$)	[m]
$\mathbf{M}$	Global mass matrix	[kg]
$\mathbf{M}_e$	Element mass matrix, global coordinate system	[kg]

Roman bold lowercase symbols

$\mathbf{f}$	Global (external) force vector	[N]
$\mathbf{f}_e$	Element (external) force vector	[N]
$\mathbf{u}$	Global displacement vector	[m]
$\mathbf{u}_e$	Element displacement vector, global coordinate system	[m]

Roman bold-italic uppercase symbols

$\boldsymbol{K}_e$	Element stiffness matrix, local coordinate system	[N/m]
$\boldsymbol{K}_e^0$	Element stiffness matrix, local coordinate system with unit Young's modulus ($E = 1$)	[m]
$\boldsymbol{M}_e$	Element mass matrix, local coordinate system	[kg]
$\boldsymbol{M}_e^0$	Element mass matrix, local coordinate system with unit mass ($m = 1$)	[-]

Roman bold-italic lower case symbols

$\boldsymbol{u}_e$	Element displacement vector, local coordinate system	[m]

Special symbols

$\max f$	Maximum (reasonable) value of objective function f
$\min f$	Minimum (reasonable) value of objective function f

Introduction

In the introduction chapter, the following symbols are used.

Roman italic lowercase symbols

x	Design variable
y	State variable

Theory

In the theory chapter, the following symbols are used.

Greek lowercase symbols

λ^l	Lagrangian multiplier, lower bound
λ^u	Lagrangian multiplier, upper bound

Greek bold lowercase symbols

$\boldsymbol{\lambda}^l$	Vector of Lagrangian multipliers, lower bound
$\boldsymbol{\lambda}^u$	Vector of Lagrangian multipliers, upper bound

Roman lowercase symbols

m_e	Element mass	[kg]
m_e^0	Element base material mass	[kg]
$m_{\min}$	Mass, lower bound	[kg]

Appendix A

In appendix A, the following symbols are used.

Greek lowercase symbols

η	Numerical damping coefficient (usually $\eta = 0.5$)
λ	Lagrangian multiplier

Roman italic uppercase symbols

B_e	Optimality criteria

Roman italic lowercase symbols

m	Move limit (usually $m = 0.2$)

Contents

1 Introduction

In this chapter the context of the topic is presented. Thereafter a brief background of structural optimization, of which topology optimization is a subfield, is given. The background is followed by the purpose and the limitations of the thesis. At the end of the chapter, an outline of the thesis is found.

1.1 Context

Our resources, both in terms of material and money, have always been limited, which spurred the desire to constantly improve the way we do things. As things are improved, we move toward a more sustainable usage of resources. We can talk of doing things optimal, that is, we apply optimization in order to determine which design is the best from different perspectives. As the computational possibilities has developed over the past decades, the interest of *structural optimization* has grown. Without going into detail, one can shortly describe structural optimization as a way of finding assemblies of materials that sustain loads in the best way. During recent years, the academical findings in the field have started to enter the commercial sphere as software manufacturers have included structural optimization modules in to their structural analysis tools.

The increase in computational power have also lead to the development of advanced computer aided design (CAD) softwares. Within the field of structural engineering and architecture MicroStation, Revit and, lately and increasingly more popular, Rhinoceros are examples of a few of these softwares. All of these enables the creation of parametric models with ease and thus possibilities to add scripting as a way to find suitable designs. Architects have been keen on using these tools and are more often talking about creating "optimized" solutions (also referred to as *performance based* design [13]). This can, however, from a mathematic point of view, be questioned; the optimal solutions discussed by architects are in most cases based on a subjective definition of optimality and not the well defined mathematical meaning of optimality. The interest amongst architects have nevertheless increased the need for structural engineers to be able to supports the design process and discuss optimum from an objective and scientific point of view.

As a response to this demand, a vast number of tools capable of performing optimization of geometries and structures have entered the market in the last few years. Some of the tools are created as a product of academical projects, however few of these are intended to increase the understanding of the underlaying concepts of the optimization. Furthermore, most of the tools are dealing with optimization of shape and size, and not with topologies. This is somewhat odd since topology optimization problem setups can give results very close to both shape and size optimization at the same time.

The interest of optimization within the built industry seams, according to the author, inexhaustible. One can also discern a growing interest in topology optimization amongst architects and engineers. Sadly, these trends are not reflected at schools teaching our engineers of tomorrow; there is a gap between the mathematical theory

and the application of optimization as a design tool. Within this context, a need for a greater understanding of the subject is appropriate in order to support this development.

1.2 Background

1.2.1 Structural Optimization

In this section, a brief overview of the topic structural optimization is given. The interested reader is recommended to have a look in the book *An Introduction to Structural Optimization* by Christensen and Klarbring [5] for a more thorough overview of structural optimization. The book *Optimization of Structural Topology, Shape and Material* by Bendsøe [3] is another good source.

Gordon [10] defines a mechanical *structure* as "any assemblage of materials which is intended to sustain loads" and *optimization* means making the best of something. Thus, together *structural optimization* means "making of an assembly of materials that sustain loads in the best way". This definition of structural optimization, presented by Christensen and Klarbring [5], is somewhat vague since "the best way" can be interpreted in many ways, e.g. to make the structure as light as possible or as stiff as possible. However, the definition suits the purpose since what is the best way varies from case to case.

Problem Classes

Structural optimization problems can be divided into three classes of which the last class of problems are the main focus of this thesis.

Size Optimization
In size optimization some size parameter of the structure is optimized. The size parameter is typically the cross section of a bar in a truss (see e.g., [13]) or the thickness distribution of a plate.

Shape Optimization
Shape optimization relates to optimize the contour of some part of the boundary of the structural domain. This type of problems are some times referred to as *form finding*, e.g. when grid strucutres or tensile structures are shape optimized (see e.g. [13, 11]).

An example of a building where shape optimization have been applied is the velodrome in London Velopark[1], see fig. 1.1.

Topology Optimization
Topology optimization problems are the most general type of structural optimization problems. The best topology – or connectivity – of a structure is sought. This is usually done by turning on or off parts of the design domain in order to meet some

[1] Pete Winslow (Senior Engineer, Expedition Engineering) at the Construction and Design seminar at Chalmers University of Technology, November 26th, 2012.

Figure 1.1: *The velodrome in London Velopark. The shape of the roof and the bowl where found through optimization where tough requirements on the indoor climate as well as structural efficiency where the the main driving objectives. Architect: Hopkins Architects. Structural engineer: Expedition Engineering. Image source [12].*

criteria of optimality related to the sought objective. If we consider the sizing of members in a truss, this form of optimization allows for the sectional thickness to take the value zero meaning the member is removed from the structure. In a similar way, holes are allowed in two dimensional structures such as plates or voids in three dimensional structures such as a solid continuum body.

Few built projects where topology optimization have played a significant role for the final design is known. A recent project conducted at the Aarhus School of Architecture in Denmark shows, however, that topology optimization in architecture is possible. Some of the results from the project where presented in an article by Dombernowsky and Søndergaard [6]. Based on the experience gained, the authors claims that the method would be beneficial to apply in larger scale, e.g. in terms of material usage and in design possibilities. An example of a structures made by the team can be seen in fig. 1.2.

General Mathematical Form of a Structural Optimization Problem

For all structural optimization problem, the *objective function* (f) usually measures the structure's weight, displacement in a given direction, effective stress, cost of production, compliance or other relevant features of the structure. The *design variable* (x) is a field or a vector field that describes the design in some way and can represent the geometry or choices of material.

Along with these two, there is a need for a *state variable* (y) in order to define the problem. The state variable is a field or a vector field that describes, for a given design x, the response of the structure on which the objective function has to react. The state function can describe the displacement, stress, strain or force and is thus

Figure 1.2: *Concrete pavilion with roof structure found using topology optimization. Image source [22].*

an implicit function of x. Such implicitly dependency of functions will be denoted by the use of curly brackets throughout the thesis.

A general structural optimization problem can be written [5]:

$$\begin{cases} \min\limits_{x,y} & f(x, y\{x\}) \\ \\ \text{subject to} & \begin{cases} \text{behavioral constrains on } y\{x\} \\ \text{equilibrium constraint} \\ \text{design constrains on } x \end{cases} \end{cases}, \tag{1.1}$$

where the behavioral constrains can be, e.g., a stress or a volume limit. This form, often referred to as a closed form, will be used through out the thesis when defining the optimization problems.

1.2.2 Multi-Objective Optimization

Multi-objective optimization problems involves optimization of multiple objective functions, f_i:s, at the same time. Such problems can, following the format presented in eq. (1.1), be written as:

$$\begin{cases} \min\limits_{x,y} & \left(f_1, f_2, \ldots, f_{n_f}\right) \\ \\ \text{subject to} & \text{constraints} \end{cases}, \tag{1.2}$$

where n_f denotes the number of objective functions, f_i:s, considered. The different objectives are often contradictory, i.e. they are generally not optimized for the same value of the design parameter. It is usually convenient to apply some kind of trick

to problems like eq. (1.2) in order be able to track the *Pareto-optimal frontier* as in fig. 1.3 and thus find *Pareto-optimality*: a design that satisfies all the objectives in such a way that it is impossible to make any one objective better off without making at least one objective worse off is called a Pareto-optimal design.

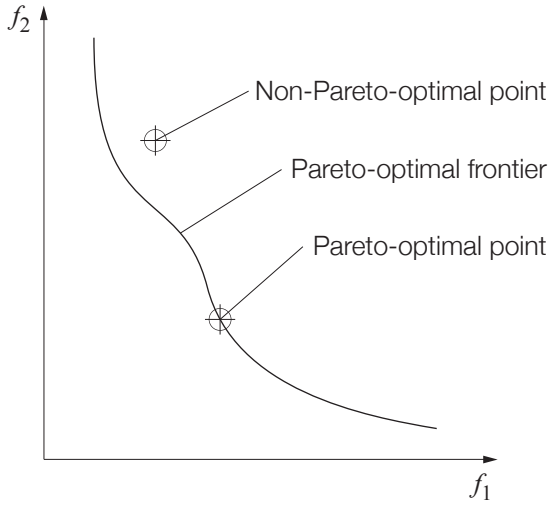

Figure 1.3: *Pareto-optimal points and Pareto-frontier for two objective functions* f_1 *and* f_2.

There are several ways to obtain the Pareto-optimality, but a common and straightforward way to do so is to merge the objective functions f_i of eq. (1.2) into a scalar objective function for which the optimization is performed:

$$\begin{cases} \min\limits_{x,y} & \sum_{i=1}^{n_f} w_i f_i, \\ \text{subject to} & \text{constraints} \end{cases}, \tag{1.3}$$

where $w_i \geq 0$ are objective weight factors whose sum is 1. Equation (1.3) is a standard scalar optimization problem that will give one Pareto-optimal point of eq. (1.2). Different Pareto-optimal points are obtained by varying the weights and thus the Pareto-optimal frontier can be constructed. However, this simple method will not in general be able to find all Pareto-optimal points [5]. A more powerful method will be presented later in the theory chapter.

1.3 Purpose

The purpose of this thesis is to propose a formulation approach and solution method for multi-objective topology optimization problems. This will enable investigation of the effect various objectives have on the optimal design obtained when performing multi-objective topology optimization. The formulation and method will be used to study the trade off between volume, compliance, and eigenvalue in structural design.

1.4 Limitations

The focus of the thesis is to solve topology optimization problems with multiple objectives formulated using a continuous parametrization formulation approach. The problems considered are limited to include linear elastic isotropic material models, i.e. problems where Hook's law applies. Furthermore the problems considered are limited to continuum structures subjected to time-independent loading and thus free vibrations.

From a theoretical point of view, there is no difference in analyzing a structure in three dimensions or in two dimensions. However, from a computational and programming perspective, three dimensional structures are much more time-consuming and complex wherefore the thesis is limited to the treatment of two dimensional structures.

1.5 Thesis outline

The report consists of a theory chapter in which the theoretical background of the formulations and algorithms used in the thesis are described. The chapter is followed by a brief overview of implementation in Matlab and Java. In the numerical examples chapter, two design problems are presented and solved. The results are compared with results obtained from single-objective topology optimization. The report is ended with a discussion together with recommendations for further work.

2 Theory

In this chapter, topology optimization is discussed in general terms but with the over all goal to be able to solve the following multi-objective topology optimization problem using a first-order gradient based solution method:

$$\begin{cases} \min\limits_{\boldsymbol{\rho},\mathbf{u}\{\boldsymbol{\rho}\}} & (V(\boldsymbol{\rho}), C(\boldsymbol{\rho}), -\lambda_1(\boldsymbol{\rho})) \\ \text{subject to} & \boldsymbol{\rho}(x) = 0 \vee 1 \quad \forall x \in \Omega \end{cases}, \tag{2.1}$$

where $V(\boldsymbol{\rho})$, $C(\boldsymbol{\rho})$ and $\lambda_1(\boldsymbol{\rho})$ are objective functions that represents the volume, compliance and lowest eigenvalue, respectively, of the structure defined by the design vector $\boldsymbol{\rho}$. The design parameter x is continuous in space and Ω is the design domain. All objectives will later be discussed in detail, however a short description of compliance is in its place to give here: compliance is in this context a scalar measure of the stiffness of the structure with respect to a specific load case; the stiffer a structure is, the lower it's compliance is.

The chapter starts with a discussion about finite element discretization of the topology optimization problem. The topology optimization formulation is thereafter discussed in terms of integer and continuos formulation approaches. This is followed by an overview of different filtering methods used to reduce the effect of numerical instabilities. Thereafter, the problem formulation is discussed in detail which enables the tracing of Pareto-optimal solutions. The chapter is ended with a description of the solution method that has been implemented.

2.1 Finite Element Discretization

The general concept of topology optimization is to determine optimal placement of a given material in space. In other words, the goal is to determine which points x should be filled with material and which points should be voids. The design parameter x is continuous in space.

However, to consider the true continuous problem is not very practical and it is convenient to discretize the problem using the finite element method, both in terms of the geometry and in terms of the design parameter. When applying finite element discretization on the design domain, we can think of the geometrical representation as pixels of black and white representing solid and void areas where the discretized design vector $\boldsymbol{\rho}$ turns pixels on or off. Given a design domain Ω of finite elements, we thus seek to find a optimal subset Ω^{mat} of elements that should be filled with material, i.e. the elements $e \in \Omega^{\text{mat}}$ for which ρ_e should be 1.

2.2 Integer and Continuous Formulations

The solid-void condition in stiffness governed topology optimization problem can be written as a modification of the Young's modulus of each element:

$$E_e(\rho_e) = \rho_e E_e^0, \qquad \rho = \begin{cases} 1 & \text{if } e \in \Omega^{\text{mat}}, \\ 0 & \text{otherwise} \end{cases}, \tag{2.2}$$

where the element design variable ρ_e turns the element Young's modulus, E_e, on or off depending on if the element e is within the subset Ω^{mat} of elements with material or not. E_e^0 is the base Young's modulus of element e.

The formulation in eq. (2.2) is a so-called *integer formulation* and is physically permissible. It would therefore be beneficial to be able to use this formulation in some way when constructing the objective function needed for the optimization. Integer formulations delimits however the possibility to use gradient based optimization algorithms, i.e. solution methods dependent of the possibility to find the derivatives of the objective function. To use these kind of methods, a *continuous formulation* is needed. A common way to achieve this is to relax the integer condition on ρ_e in eq. (2.2) allowing ρ_e to take any value between 0 and 1 and at the same time introduce some kind of penalty for intermediate values. The penalty means it will be more expensive to take a value between 0 and 1 than it is to take an integer value when comparing the stiffness to the weight as a function of ρ_e. Doing so transforms the topology optimization into a sizing optimization problem dependent on the – now continuous – design parameter ρ_e; we will now try to find the optimal "size" of ρ_e.

From this follows that we can interpret the design variables ρ_e as a *generalized density* or a *virtual density*. This is however not physically permissible since no homogenous material exists where we can vary the density as we like. This problem can be resolved, e.g. by fulfilling the so-called Hashin-Shtrikman bounds which couples the properties of a two-phase isotropic material with the properties one can achieve by constructing a composite [4].

There are several continuous interpolations for the intermediate values of ρ_e in topology optimization problems. Some of these are listed below:

- Solid Isotropic Material with Penalization (SIMP)
- Modified Solid Isotropic Material with Penalization (ModSIMP)
- Optimal Microstructure with Penalization (OMP)
- Non-Optimal Microstructures *or* Near Optimal Microstructures (NOM)
- Rational Approximation of Material Properties (RAMP)

All of these approaches have advantages and disadvantages. Rozvany discusses and evaluates some of these and claims that the SIMP approach is suitable for the common problem of minimizing the compliance [14]. In the SIMP approach, the design variable ρ_e is given a lower bound slightly larger than zero. This bound leads to some drawbacks when it comes to the solution methods which are resolved in the ModSIMP approach. The SIMP and the ModSIMP interpolation schemes are presented in the following sub sections. Further drawbacks of the SIMP schemes are related to dynamic problems (as will be explained later) which can be overcome using the RAMP interpolation scheme instead.

2.2.1 SIMP Interpolation Scheme

One possible continuous and widely implemented formulation approach that makes use of the penalization concept is the so-called *Solid Isotropic Material with Penalization*

(SIMP) interpolation scheme [4]:

$$E_e(\rho_e) = \rho_e^p E_e^0, \qquad 0 < \rho_{\min} \leq \rho_e \leq 1, \tag{2.3}$$

where p is the penalization power. The small positive constant $\rho_{\min}$ is introduced in order to prevent singularities when working with finite element discretization.

Figure 2.1a shows Young's modulus plotted against the design variable for various values of the penalization power p. As seen, the penalization power has to be grater than one in order for the penalization to take effect. For $p > 1$, intermediate values of ρ_e will contribute disproportionally low to the stiffness compared with the contribution to the weight: these values of ρ_e will be more costly than the integer values, thus intermediate values will be avoided during optimization.

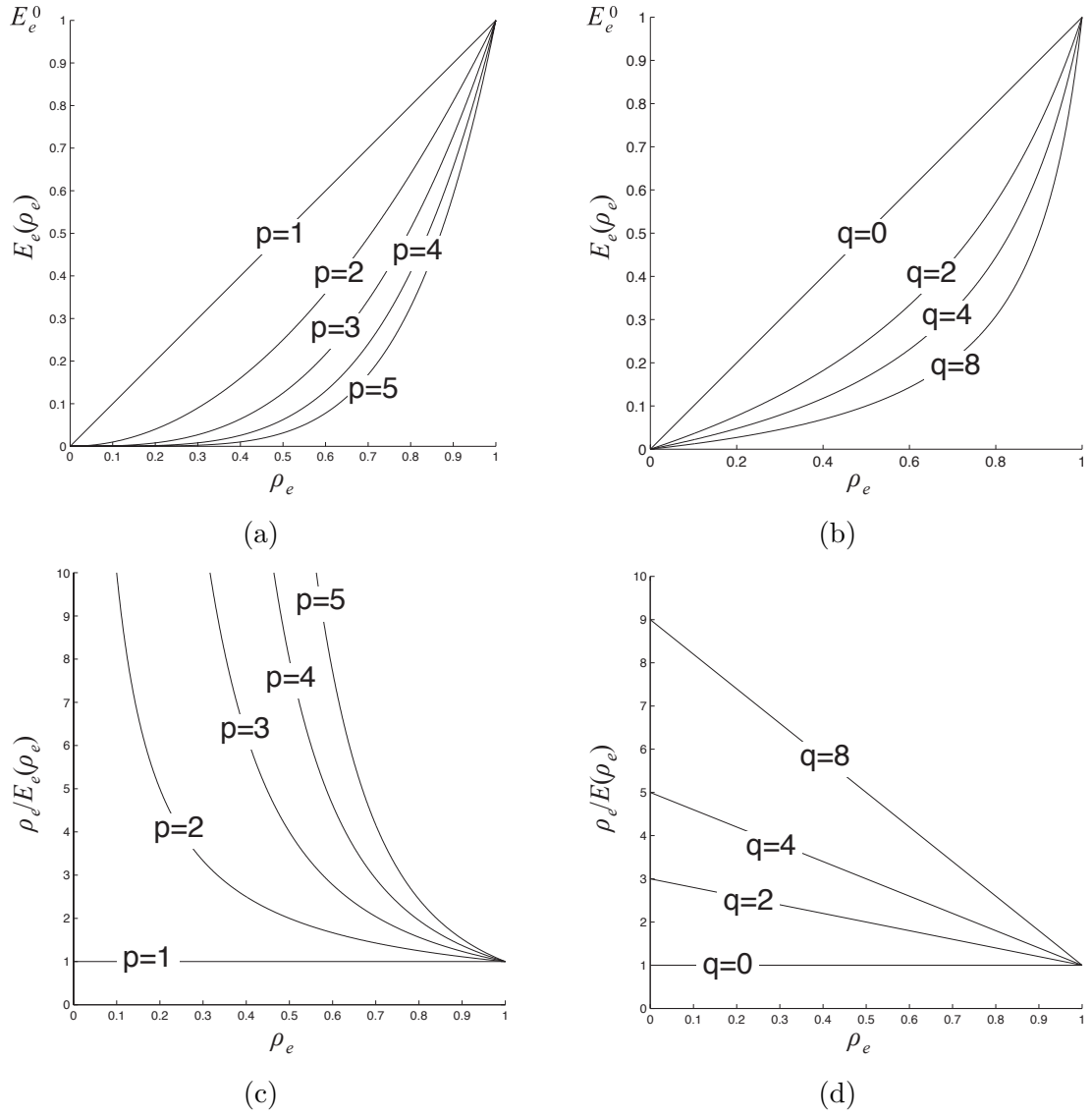

Figure 2.1: *The Young's modulus $E_e(\rho_e)$ as a function of the design parameter ρ_e for (a) the SIMP/ModSIMP and (b) the RAMP interpolation schemes for different values of the interpolation parameters p and q and corresponding mass to stiffness ratio for (c) the SIMP/ModSIMP and (d) the RAMP interpolation schemes.*

Penalization Power

As noted previously, the physical relevance of continuous formulations can be questioned; how should areas of various shades of gray be interpreted? Bendsøe and Sigmund discussed this issue and claims that the physical permissibility can be ensured as long as some conditions on the penalization power are satisfied [2]:

$$p \geq \max\left\{\frac{2}{1-\nu^0}, \frac{4}{1+\nu^0}\right\} \qquad \text{(2D-case)}, \tag{2.4a}$$

$$p \geq \max\left\{15\frac{1-\nu^0}{7-5\nu^0}, \frac{3}{2}\frac{1-\nu^0}{1-2\nu^0}\right\} \qquad \text{(3D-case)}, \tag{2.4b}$$

where ν^0 is the Poisson's ratio for the base material with stiffness E^0. The condition is based on the Hashin–Shtrikman bounds for two-phase materials making it possible to interpret the stiffness obtained using the SIMP scheme as the stiffness of a composite consisting of voids and the base material. For the common case $\nu^0 = 1/3$, $p \geq 3$ in both 2D and 3D.

2.2.2 ModSIMP Interpolation Scheme

The *Modified Solid Isotropic Material with Penalization (ModSIMP)* interpolation scheme is based on the same principles as the SIMP scheme and penalizes intermediate values of the design variable ρ_e:

$$E_e(\rho_e) = E_{\min} + \rho_e^p(E_e^0 - E_{\min}), \qquad 0 \leq \rho_e \leq 1, \tag{2.5}$$

where $E_{\min}$ is a very small stiffness assigned to void elements in order to avoid singularities associated with the finite element discretization. $E_{\min}$ has thus the the same purpose as $\rho_{\min}$ in eq. (2.3). The penalization power p is selected in the same way as for the SIMP interpolation scheme, i.e. eq. (2.4) applies.

Since the ModSIMP interpolation scheme allows ρ_e to take the value 0, it has several advantages compared with the SIMP interpolation scheme. The most important being the possibility of straightforward implementation of additional filters [19].

2.2.3 RAMP Interpolation Scheme

The SIMP and ModSIMP interpolation schemes are well suited for solving stiffness optimization problems. However, applying these schemes on eigenvalue optimization problems may lead to the appearance of "artificial modes". These appear as highly localized modes in areas of the structure with a large mass to stiffness ratio. For the SIMP schemes this happens as the generalized density goes to zero, which is seen in fig. 2.1c. Low density regions thus give rise to low eigenfrequencies. To resolve this, one has to use an interpolation scheme that makes sure that the mass to stiffness ratio always is finite as the generalized density vanishes ($\rho_e \to 0$) [4]. Such a interpolation scheme is the *Rational Approximation of Material Properties (RAMP)* interpolation scheme:

$$E_e(\rho_e) = E_{\min} + \frac{\rho_e}{1+q(1-\rho_e)}(E_e^0 - E_{\min}), \qquad 0 \leq \rho_e \leq 1, \tag{2.6}$$

where $q \geq 0$. The scheme is depicted in fig. 2.1b for various choices of q and the corresponding mass to stiffness ratio in fig. 2.1d.

For choices of $q \geq \bar{q}$, $\bar{q} \equiv (E_e^0 - E_{\min})/E_{\min}$, the RAMP scheme makes by it's construction the compliance a concave function of ρ_e. For materials with Poisson's ratio $\nu^0 = 1/3$, the Hashin–Shtrikman lower bound is fulfilled for

$$q \geq 2\frac{E_e^0 - E_{\min}}{E_e^0 - 2E_{\min}}, \tag{2.7a}$$

$$q \leq \frac{2(E_e^0 - E_{\min})}{3E_{\min}}. \tag{2.7b}$$

The first order derivative of the RAMP interpolation scheme:

$$\frac{\partial E_e}{\partial \rho_e} = \frac{1+q}{(1+q(1-\rho_e))^2}(E_e^0 - E_{\min}), \tag{2.8}$$

is always grater than zero for all choices of $q \geq 0$, a feature the SIMP schemes do not have which for $\rho_e = 0$ has a zero derivative. This implies that the SIMP schemes will never satisfy the Hashin-Shtrikman bounds for all densities whereas the RAMP scheme always will do so if q is selected within the bounds [21].

It should however be noted that the lower bound, eq. (2.7a), in general do not ensure a concave compliance with respect to the design variables [21].

2.3 Filter

The usage of integer or continuous formulation approaches does not first and foremost guarantee an existence of a solution to the optimization problem. Nor does the approaches bound the number of voids or, in 3D, limits the thickness of a design solution. Furthermore, numerical oscillations in the design leading to a so-called *checkerboard patterns* may occur in which the design ρ_e alternates between solid and void in some regions of the solution causing patterns similar to the one in fig. 2.2. Such structures can not transfer any load since the solid elements are not in connection with each other other than in their vertices, which are infinitesimal.

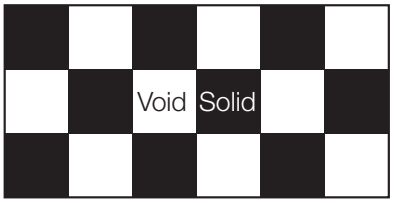

Figure 2.2: *Checkerboard pattern: alternation between solids and voids. Each square is an element.*

All of these issues are well established phenomenas [4]. Apart from being a theoretical drawback, this makes the results sensitive to the resolution of the finite element mesh. These issues can be resolved by several means [18] of which the application of a filter is a common choice. A filter relates the design of each element to the design of the other elements in some way. Mesh independent filters, see fig. 2.3, based on filtering of sensitivities or density are commonly used, much due to their simplicity.

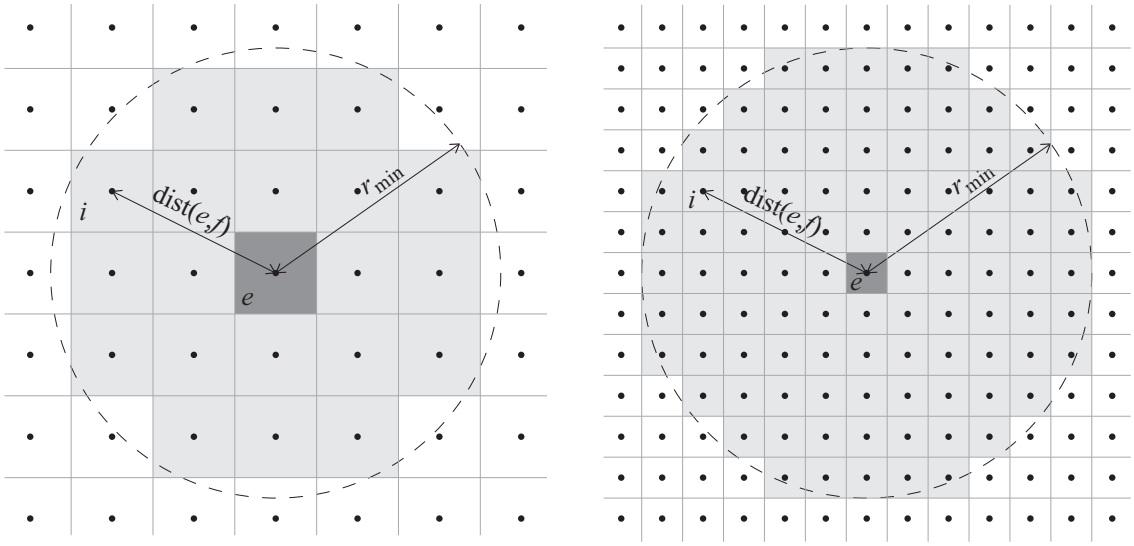

Figure 2.3: *Example of mesh independent filter principle. The filter area for element e is bounded by the perimeter of a circle with radius* $r_{\min}$*. Due to discretization into elements, only the shaded elements contributes to the filter since these elements have their centroid within the filter area. Note that the filter works the same way in the 3D-case, however the filter area is then a filter volume bounded by the perimeter of a sphere with radius* $r_{\min}$*.*

2.3.1 Sensitivity Filter

A sensitivity filter, which perhaps is the most popular filter, was proposed by Sigmund in 1997 [20]. It works by modifying the sensitivities of each element relating it's sensitivity to the weighted mean of the sensitivity with respect to the densities of the elements in a fixed neighborhood:

$$\widehat{\frac{\partial f}{\partial \rho_e}} = \frac{1}{\max(\gamma, \rho_e) \sum\limits_{i \in N_e} H_{ei}} \sum_{i \in N_e} H_{ei} \rho_i \frac{\partial f}{\partial \rho_i}, \tag{2.9}$$

where f is the objective function the filter is applied on, N_e is the set of elements i for which the Euclidian centre-to-centre distance, $\text{dist}(e, i)$, is smaller than the filter radius $r_{\min}$. The weight factor is defined as:

$$H_{ei} = \max(0, r_{\min} - \text{dist}(e, i)). \tag{2.10}$$

The term γ $(= 10^{-3})$ is a small number introduced in order to avoid division by zero needed when ρ_e has 0 as it's lower bound. From this definition follows that the weight factor is zero outside the filter area and that it decreases linearly with an increased distance from the centroid of element e.

2.3.2 Density Filter

The density filter works by modifying the generalized densities as follows [1]:

$$\tilde{\rho}_e = \frac{1}{\sum\limits_{i \in N_e} H_{ei}} \sum_{i \in N_e} \rho_i H_{ei}. \tag{2.11}$$

Since this means a modification of the actual design parameter, the sensitivities of the various objectives with respect to the densities of the elements, ρ_j, needs to be modified using the chain rule [1]:

$$\frac{\partial f}{\partial \rho_j} = \sum_{e \in N_j} \frac{\partial f}{\partial \tilde{\rho}_e} \frac{\partial \tilde{\rho}_e}{\partial \rho_j} = \sum_{e \in N_j} \frac{1}{\sum\limits_{i \in N_e} H_{ei}} H_{je} \frac{\partial f}{\partial \tilde{\rho}_e}. \tag{2.12}$$

The benefit of the density filter compared to the sensitivity filter is the remained connection between the design parameter and the derivative with respect to the design parameter. When approximations are introduced, as will be seen later when the solution method is discussed, it is crucial to have this connection. Otherwise, the update in each iteration will not fit with the evaluated design; the design and the update, based on the derivative, would not represent the same structure.

2.4 Continuation Method

Even though filters are used, numerical instabilities may still be a problem. These can be reduced by the use of continuation methods which are based on the idea of gradually go from an artificial convex problem to the try non convex problem in a number of steps [18]. The continuation method can e.g. be applied on the interpolation parameter which is increased in each continuation step or the filter radius which is decrease in each continuation step. Figure 2.4 shows a schematic overview of the method.

2.5 Problem Formulation

In this section, the problem formulation of the multi-objective topology optimization problem presented in eq. (2.1) at the beginning of this chapter will be discussed in detail. Recall eq. (2.1):

$$\begin{cases} \min\limits_{\boldsymbol{\rho}, \mathbf{u}\{\boldsymbol{\rho}\}} & (V(\boldsymbol{\rho}), C(\boldsymbol{\rho}), -\lambda_1(\boldsymbol{\rho})) \\ \text{subject to} & \boldsymbol{\rho}(x) = 0 \vee 1 \quad \forall x \in \Omega \end{cases},$$

By applying finite element discretization and using a continuous interpolation formulation approach for intermediate values of design parameters ρ_e, the problem can be written as:

$$\begin{cases} \min\limits_{\boldsymbol{\rho}, \mathbf{u}\{\boldsymbol{\rho}\}} & (V(\boldsymbol{\rho}), C(\boldsymbol{\rho}), -\lambda_1(\boldsymbol{\rho})) \\ \text{subject to} & \mathbf{0} \leq \boldsymbol{\rho} \leq \mathbf{1} \end{cases}, \tag{2.13}$$

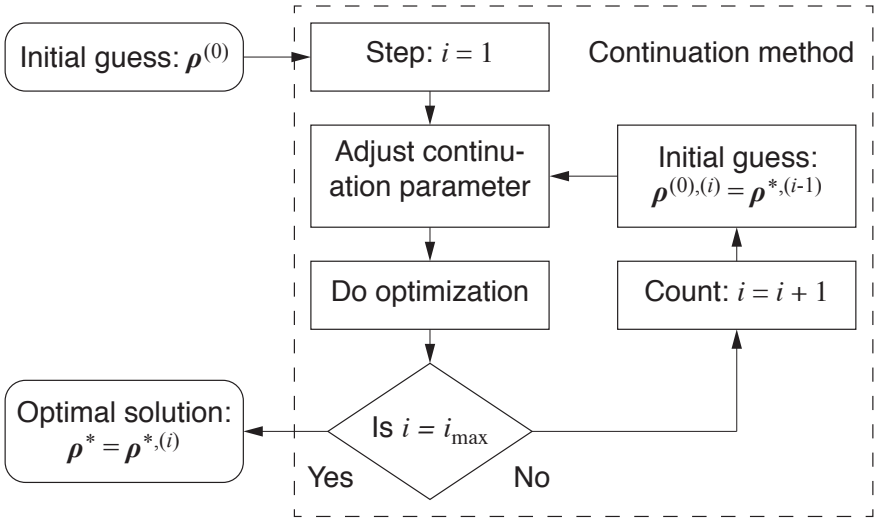

Figure 2.4: *Schematic overview of the continuation method where $i_{\max}$ is the number of maximum allowed continuation steps. In each continuation step i, the continuation parameter is adjusted. In case the continuation parameter is the filter radius, the parameter adjustment can e.g. be $r = (i_{\max} - i)r_{\min}$ implying that for $i = i_{\max}$ we have $r = r_{\min}$.*

As noted previously in section 1.2.2, this formulation is not a convenient way to handle the problem; there are few solution methods that can handle several different objectives concurrently. This will be handled using *compromise programming* as described in a subsequent sub-section. Firstly, however, the objective functions themselves will be discussed as the formulation of these are not trivial, especially when it comes to the compliance and the eigenvalue.

2.5.1 Objective Functions

Volume

The volume objective, measured in [m^3], is linearly dependent on $\boldsymbol{\rho}$:

$$V(\boldsymbol{\rho}) = \sum_{e=1}^{n_{el}} \rho_e V_e^0, \tag{2.14}$$

and has the following derivative with respect to the design parameters ρ_e:

$$\frac{\partial V(\boldsymbol{\rho})}{\partial \rho_e} = V_e^0, \tag{2.15}$$

where V_e^0 is the base volume of each element.

Compliance

The compliance is a way to describe the stiffness of a structure with respect to a specific load case: the stiffer the structure is, the lower the compliance is. It is a

scalar measure and is here formulated as:

$$C(\boldsymbol{\rho}) = \mathbf{f}(\boldsymbol{\rho})^{\mathrm{T}}\mathbf{u}\{\boldsymbol{\rho}\} = \sum_{e=1}^{n_{el}} E_e(\rho_e)\boldsymbol{u}_e^{\mathrm{T}}\boldsymbol{K}_e^0\boldsymbol{u}_e, \tag{2.16}$$

where $\boldsymbol{K}_e^0$ is the element stiffness matrix in local coordinate system with unit Young's modulus ($E = 1$ [-]). The derivative of the compliance is:

$$\frac{\partial C(\boldsymbol{\rho})}{\partial \rho_e} = -\frac{\partial E_e}{\partial \rho_e}\boldsymbol{u}_e^{\mathrm{T}}\boldsymbol{K}_e^0\boldsymbol{u}_e. \tag{2.17}$$

The element displacement in local coordinate system, $\boldsymbol{u}_e \equiv \boldsymbol{u}_e\{\boldsymbol{\rho}\}$, is found solving the global displacements $\mathbf{u} \equiv \mathbf{u}\{\boldsymbol{\rho}\}$ in $\mathbf{K}(\boldsymbol{\rho})\mathbf{u}\{\boldsymbol{\rho}\} = \mathbf{f}(\boldsymbol{\rho})$ where $\mathbf{f}(\boldsymbol{\rho})$ is the global load vector, and then transforming the relevant partition of $\mathbf{u}$ into local coordinates. The stiffness matrix is found as

$$\mathbf{K}(\boldsymbol{\rho}) = \sum_{e=1}^{n_{el}} E_e(\rho_e)\mathbf{K}_e^0, \tag{2.18}$$

where $\mathbf{K}_e^0$ is the element stiffness matrix in global coordinate system with unit Young's modulus.

A more thorough discussion on the derivation of the compliance can be found in appendix A.

Eigenvalue

The lowest eigenvalue of the structure, $\lambda_1 \equiv \lambda_1(\boldsymbol{\rho})$, under free vibration and the corresponding eigenvector, $\boldsymbol{\phi}_1 = \left[\boldsymbol{\phi}_1^{\text{fixed}}, \boldsymbol{\phi}_1^{\text{free}}\right]$ with $\boldsymbol{\phi}_1^{\text{fixed}} = \mathbf{0}$, are found by solving $\left[\mathbf{K}^{\text{free}}(\boldsymbol{\rho}) - \lambda_1\mathbf{M}^{\text{free}}(\boldsymbol{\rho})\right]\boldsymbol{\phi}_1^{\text{free}} = \mathbf{0}$ [1]. The sensitivity of the lowest eigenvalue is thereafter found as [8]:

$$\frac{\partial \lambda_1}{\partial \rho_e} = \boldsymbol{\phi}_1^{\mathrm{T}}\frac{\partial \mathbf{K}(\boldsymbol{\rho})}{\partial \rho_e}\boldsymbol{\phi}_1 - \lambda_1\boldsymbol{\phi}_1^{\mathrm{T}}\frac{\partial \mathbf{M}(\boldsymbol{\rho})}{\partial \rho_e}\boldsymbol{\phi}_1, \tag{2.19}$$

where $\mathbf{K}$ and $\mathbf{M}$ is the global stiffness and mass matrix, respectively. The mass matrix is found as

$$\mathbf{M}(\boldsymbol{\rho}) = \sum_{e=1}^{n_{el}} m_e(\rho_e)\mathbf{M}_e^0, \tag{2.20}$$

where $\mathbf{M}_e^0$ is the element mass matrix in global coordinate system with unit mass ($m = 1$ [-]). The element mass is found as $m_e(\rho_e) = m_{\min} + \rho_e(m_e^0 - m_{\min})$ where m_e^0 is the element base mass and the small mass m_{min} is introduced in order to avoid singularities in the $\mathbf{M}$-matrix (c.f. the meaning of $E_{\min}$ in the ModSIMP and RAMP interpolation schemes for the $\mathbf{K}$-matrix).

The derivatives of the stiffness and mass matrix are then

$$\frac{\partial \mathbf{K}(\boldsymbol{\rho})}{\partial \rho_e} = \frac{\partial E_e}{\partial \rho_e}\mathbf{K}_e^0, \tag{2.21}$$

[1] In Matlab the system is preferably solved using the the command `[V,D]=eigs(K_free, M_free, k, 'sm')` where `k` specifies the number of sought eigenvalues and `'sm'` specifies that the eigenvalues with the smallest magnitude are sought.

and

$$\frac{\partial \mathbf{M}(\boldsymbol{\rho})}{\partial \rho_e} = \frac{\partial m_e}{\partial \rho_e}\mathbf{M}_e^0, \tag{2.22}$$

respectively.

It should be noted that eq. (2.19) only holds if λ_1 is a distinct eigenmode – or *single* modal – [4], i.e. there exists no other eigenvalues λ_i such that $\lambda_i = \lambda_1$ and $\boldsymbol{\phi}_i \neq \boldsymbol{\phi}_1$. If that is the case, usually appearing in symmetric structures, one has to use other means in order to find the eigenvalue sensitivity (see e.g. [16]). The need for such consideration has not been necessary in this thesis since all computed eigenvalues have been single modal; in the code implemented to solve the optimization problem, a check is done each time λ_1 is calculated and the program throws an error and stops executing if λ_1 is not single modal.

2.5.2 Compromise Programming

The formulation of eq. (2.13), with it's several objectives, is not suitable for standard gradient based optimization algorithms. A straightforward way to handle the problem is to make use of Pareto optimality where all objectives are merged into a global objective function using weights (recall eq. (1.3)). We then only get one function to minimize and can track the Pareto-optimal frontier by adjusting the weight factors w_i. The merging has, however, to be done in a clever way and not just by summing the objectives. Otherwise there is a risk that objectives with very different appearance will be incompatible resulting in difficulties of finding various solutions regardless of what weights are used. To overcome this, the objectives can be made dimensionless and scaled in order to ensure the objectives have the same magnitude.

A formulation that make use of this concept is called compromise programming [15]. Compromise programming combines weighing and dimensionless scaling as well as applies a norm to the result. Following this formulation approach, eq. (2.1) is transformed into:

$$\begin{cases} \min\limits_{\boldsymbol{\rho}} & l_p(\boldsymbol{\rho}) \\ \text{subject to} & \mathbf{0} \leq \boldsymbol{\rho} \leq \mathbf{1} \end{cases}, \tag{2.23}$$

where $l_p(\boldsymbol{\rho})$ is the global function or *compromise* defined as:

$$l_p(\boldsymbol{\rho}) = \left[\sum_{i=1}^{n_f} w_i^{p_n} \left(\frac{f_i(\boldsymbol{\rho}) - \min f_i}{\max f_i - \min f_i}\right)^{p_n}\right]^{(1/p_n)}, \tag{2.24}$$

where w_i are the weight factors, $\min f_i$ and $\max f_i$ is the minimal and maximal value, respectively, of objective i (suggested values for theses will be discussed in the following section); $f_i(\boldsymbol{\rho})$ is the objective value of the i:th objective (that is minimized). For $p_n = 1$ the formulation turns into the weighting method with scaling and for $p_n \to \infty$ the formulation turns into the minimax approach. In-between, i.e. $2 \leq p_n < \infty$, the larger values in the parenthesis carry grater weights. In case the objective f_i is not supposed to be minimized but instead to be maximized, the expression within the parenthesis has to be changed from

$$\frac{f_i(\boldsymbol{\rho}) - \min f_i}{\max f_i - \min f_i}, \tag{2.25}$$

to

$$\frac{\max f_i - f_i(\boldsymbol{\rho})}{\max f_i - \min f_i}. \tag{2.26}$$

The derivative of eq. (2.24) is:

$$\begin{aligned}\frac{\partial l_p(\boldsymbol{\rho})}{\partial \rho_e} &= \left[\sum_{i=1}^{n_f} w_i^{p_n}\left(\frac{f_i(\boldsymbol{\rho}) - \min f_i}{\max f_i - \min f_i}\right)^{p_n}\right]^{(1/p_n - 1)} \times \\ &\times \left(\sum_{i=1}^{n_f} \frac{w_i^{p_n}\dfrac{\partial f_i(\boldsymbol{\rho})}{\partial \rho_e}\left(\dfrac{f_i(\boldsymbol{\rho}) - \min f_i}{\max f_i - \min f_i}\right)^{p_n - 1}}{\max f_i - \min f_i}\right).\end{aligned} \tag{2.27}$$

Scaling

The scaling of the objective functions is controlled via the $\min f_i$ and $\max f_i$ values. The values can be selected according to the equations below, involving solving a single-objective topology optimization problem:

$$\max C = \begin{cases} \min\limits_{\boldsymbol{\rho}} & C(\boldsymbol{\rho}) \\ \text{subject to} & \begin{cases} \dfrac{V(\boldsymbol{\rho})}{V_\Omega} = f_{V,\min} \\ \mathbf{0} \leq \boldsymbol{\rho} \leq \mathbf{1} \end{cases} \end{cases}, \tag{2.28a}$$

$$\min C = C(\mathbf{1}), \tag{2.28b}$$

$$\min \lambda_1 = \lambda_1(\boldsymbol{\rho}_{\max C}), \tag{2.28c}$$

$$\max \lambda_1 = 1.5\lambda_1(\mathbf{1}), \tag{2.28d}$$

$$\min V = V_\Omega f_{V,\min}, \tag{2.28e}$$

$$\max V = V_\Omega, \tag{2.28f}$$

where $\boldsymbol{\rho}_{\max C}$ is the design variables obtained when finding $\max C$. The optimization problem related to finding $\max C$ is solved e.g. in accordance with appendix A.

The volume fraction $f_{V,\min}$ is the smallest reasonable volume fraction of the problem set-up at hand (mesh, boundary conditions, loads). This parameter should be selected with care, which can be illustrated by studying the compromised value $l_p(\boldsymbol{\rho})$ for a set of weight factors ($w_C = \{1.0, 0.9, \ldots, 0\}$, $w_V = \{0, 0.1, \ldots, 1.0\}$ and $w_{\lambda_1} = 0$) obtained for the structure setup defined in fig. 2.5. The force is set to $P = 1$ N, the base material has Young's modulus $E^0 = 1$ Pa and Poisson's ratio $\nu^0 = 0.3$. The ModSIMP penalization power is set to $p = 3$ and the compromise norm $p_n = 1$.

By assigning all elements the same generalized density (no optimization is done) and varying the choice of the smallest reasonable volume fraction $f_{V,\min}$, the plots in fig. 2.6 are obtained. In these plots it can be seen that small volume fractions (fig. 2.6a) causes $\max C$ to be very large since $C(\boldsymbol{\rho}) \to \infty$ as $f_{V,\min} \to 0 \Rightarrow \boldsymbol{\rho} \to \mathbf{0}$, which in turn leads to clustering of the minima points of the various curves around

the same point ($\rho_e \approx 0$). From this follows that if an optimization would be done using a very low volume fraction, one would expect all Pareto-optimal solutions to be the same with a mean density of $\rho_e \approx 0$, i.e. no structure would be present (which is of course not what is desired). Several different Pareto-optimal designs would instead be expected if the minima points where distributed along the horizontal axis as in figs. 2.6b to 2.6d.

The distribution should however make sense to the studied structure. Using $f_{V,\min} = 0.1$ as the smallest reasonable volume fraction results in almost evenly distributed minima points (fig. 2.6c) whereas volume fractions both larger and smaller than 0.1 results in uneven distributions along the horizontal axis (figs. 2.6b and 2.6d). It should be stressed that the suitable choice of the smallest reasonable volume fraction $f_{V,\min}$ is problem specific.

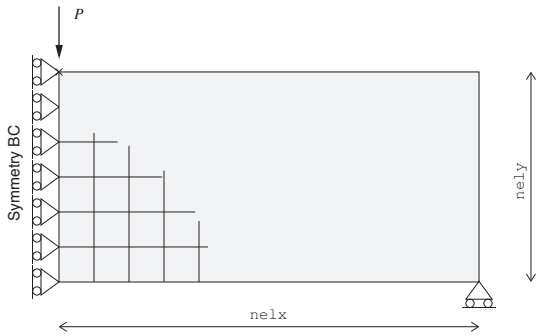

Figure 2.5: *Half of an Messerschmitt-Bolkow-Blohm (MBB) beam modeled with* $\texttt{nelx} \times \texttt{nely}$ *square Melosh elements loaded with a force* P*.*

2.6 Solution Methods

To solve problems like eq. (2.13) one can apply several solution methods depending on what constraints are present and what the cost of evaluating the objective function is. The solution methods often rely on non-linear programming algorithms. The problems to solve are usually large and therefore computationally expensive. Solution methods that needs few evaluations of the objective in order to find the optimal solution are thus favorable. Such solution methods are for instance gradient based methods. For the considered problem, the second order derivative expressions are tricky to find and the evaluation cost is increased a small portion if the second order derivatives are to be computed, thus a first-order gradient based solution method will be applied.

To solve single-objective topology optimization problems under volume constraints, the *optimality criteria method (OC)* is convenient to use [3]. The method is based on Lagrangian multipliers and a more detailed description of the method together with literature references can be found in appendix A. However, since there is no volume constraint in eq. (2.23), the presented OC method cannot be applied in order to solve the problem.

For such problems, one can make use of sequential linear programming (SLP)

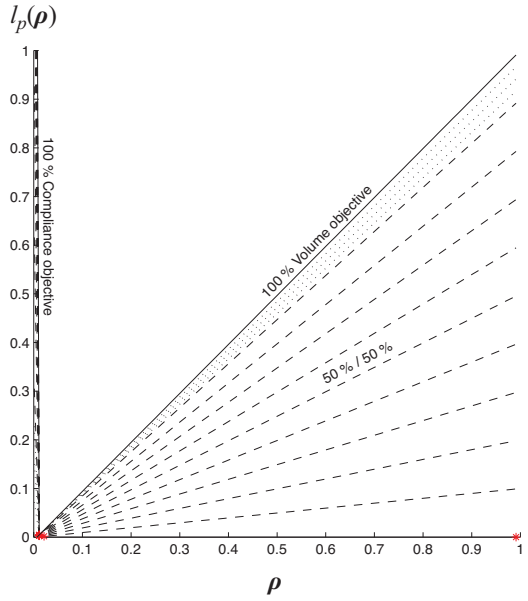

(a) $f_{V,\min} \to 0 \Rightarrow \max C = 10^{10}$

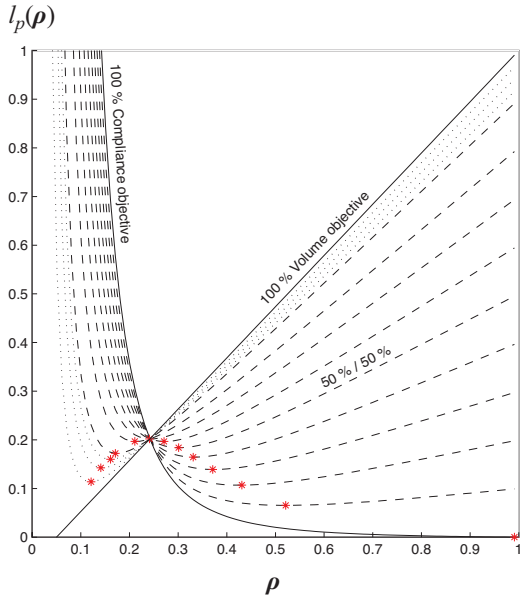

(b) $f_{V,\min} = 0.05 \Rightarrow \max C = 10\,727$

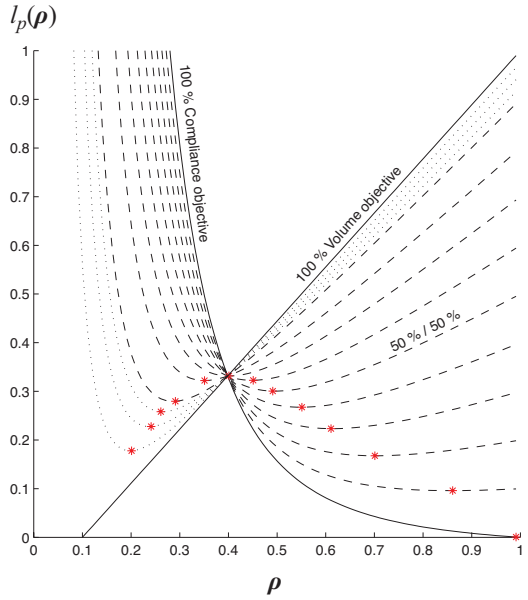

(c) $f_{V,\min} = 0.1 \Rightarrow \max C = 1\,417$

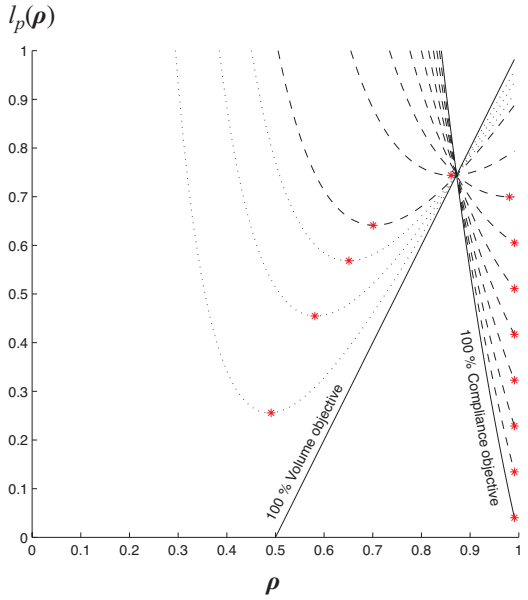

(d) $f_{V,\min} = 0.5 \Rightarrow \max C = 52$

Figure 2.6: *Compromise value $l_p(\boldsymbol{\rho})$ for volume and compliance objectives for a MBB beam made of 32×20 elements with minima points marked. The straight solid line represents full weight on volume and the curved solid line represents full weight on compliance. Each dashed and dotted line represents a 10 and 2.5 percentage points change, respectively, in the weighing between volume and compliance.*

algorithms. SLP algorithms solves non-linear problems by the use of first-order approximations, i.e. linearization, of the problem in each iteration and do not require the second-order derivatives. This causes each iteration to be relatively cheap, thus the class of methods is well suited for solving large non-linear problems.

An SLP algorithm that is globally convergent is presented in [9]. By globally convergent means that the algorithm will, from any given starting point, give a sequence of points that converges towards the set of Karush–Kuhn–Tucker (KKT) points (local minima). The algorithm handles bounded non-linear problems with non-linear equality constraints. Due to the linearization of the gradient in each step, it is important to keep a connection between the design variables and the derivatives to ensure a good approximation of the true behavior. From this follow that the sensitivity filter is disqualified as it only modifies the sensitivities and not the parameters themselves. Using the density filter and removing parts in the algorithm related to handling in-equality constraints (none are present in eq. (2.23)), the SLP algorithm can be reduced into algorithm 1 (see page 21) where $\mathcal{F}_d\langle\bullet\rangle$ and $\partial\mathcal{F}_d\langle\bullet\rangle$ denotes the application of the density filter according to eq. (2.11) and eq. (2.12), respectively.

As stopping criterion, a limit is set on the step length: stop if $\|\mathbf{s}_c\| < 10^{-9}$. Thus, the algorithm will stop executing when the difference between $\tilde{\boldsymbol{\rho}}^{(k)}$ and $\tilde{\boldsymbol{\rho}}^{(k+1)}$ is almost non-existent. Note that it is superfluous to check whether or not the point obtained when the algorithm stopped is a minima point since the algorithm is globally convergent. However, such a test is easy to implement as long as design parameter constraints, $\mathbf{0} \leq \boldsymbol{\rho} \leq \mathbf{1}$ — the so-called KKT-conditions, are taken into account. This is done by writing the Lagrangian of the problem in eq. (2.23):

$$\mathcal{L}(\boldsymbol{\rho}, \boldsymbol{\lambda}^l, \boldsymbol{\lambda}^u) = l_p(\boldsymbol{\rho}) - (\boldsymbol{\lambda}^l)^{\mathrm{T}}\boldsymbol{\rho} + (\boldsymbol{\lambda}^u)^{\mathrm{T}}(\boldsymbol{\rho} - \mathbf{1}). \tag{2.29}$$

From this follows that, for an optimal solution $\boldsymbol{\rho}^*$, the following is a necessary condition:

$$\begin{cases} \mathcal{L}'_{\boldsymbol{\rho}} &= \nabla l_p(\boldsymbol{\rho}^*) - \boldsymbol{\lambda}^l + \boldsymbol{\lambda}^u = 0, \\ \lambda^l_e \rho_e &= 0 \quad \forall e, \\ \lambda^u_e(\rho_e - 1) &= 0 \quad \forall e, \end{cases} \tag{2.30}$$

where $\boldsymbol{\lambda}_i \geq \mathbf{0}$. Since the upper and lower bounds never will be active at the same time, the following should hold for all elements e if optimality is found:

$$\begin{cases} \text{if} \quad \rho_e = 0 \;\Rightarrow\; \left\{ \begin{array}{rcl} \lambda^l_e &=& \dfrac{\partial l_p(\boldsymbol{\rho}^*)}{\partial \rho_e}, \\ \lambda^u_e &=& 0 \end{array} \right\} & \\ \text{else if} \quad \rho_e = 1 \;\Rightarrow\; \left\{ \begin{array}{rcl} \lambda^l_e &=& 0, \\ \lambda^u_e &=& -\dfrac{\partial l_p(\boldsymbol{\rho}^*)}{\partial \rho_e}, \end{array} \right\} & \text{“active” set} \\ \text{else} \quad \lambda^l_e = \lambda^u_e = 0 \;\Rightarrow\; \dfrac{\partial l_p(\boldsymbol{\rho}^*)}{\partial \rho_e} \approx 0, & \text{“inactive” set} \end{cases}, \tag{2.31}$$

where the approximation sign is related to the stopping criteria. The optimality of the obtained design can thus be checked by investigating the norm:

$$\left\| (\nabla l_p(\boldsymbol{\rho}^*))^{\text{inactive}} \right\|, \tag{2.32}$$

where $(\nabla l_p(\boldsymbol{\rho}^*))^{\text{inactive}}$ is the partition of $\nabla l_p(\boldsymbol{\rho}^*)$ where the KKT-conditions are inactive, i.e. $\forall e$ where $\lambda_e^l = \lambda_e^u = 0$.

It should be noted that it would be more accurate to check the norm of all derivatives, not only considering the inactive set. However, such consideration requires the computation of the Lagrangian multipliers, λ_e^l and λ_e^u, which would increase the computational cost.

Algorithm 1 SLP algorithm

Require: Initial guess $\boldsymbol{\rho}^{(0)}$

$j = 0$, $N = 1$, $\theta_0 = \theta_{\max} = 1$, $\delta_0 = 1$, $\delta_{\min} = 10^{-12}$

$\tilde{\boldsymbol{\rho}}^{(0)} \leftarrow \mathcal{F}_d\left\langle \boldsymbol{\rho}^{(0)} \right\rangle$

$\mathbf{g} \leftarrow \partial\mathcal{F}_d\left\langle \nabla l_p(\tilde{\boldsymbol{\rho}}^{(0)}) \right\rangle$

while a stopping criterion is not satisfied **do**

Determine $\mathbf{s}_c$, the solution of:

$$\begin{cases} \min & \mathbf{g}^{\mathrm{T}}\mathbf{s} \\ \text{s.t.} & \mathbf{s}_l \leq \mathbf{s} \leq \mathbf{s}_u \end{cases},$$

where $\mathbf{s}_l = \max\left(-\delta_j, \boldsymbol{\rho}_l - \boldsymbol{\rho}^{(j)}\right)$ and $\mathbf{s}_u = \min\left(-\delta_j, \boldsymbol{\rho}_u - \boldsymbol{\rho}^{(j)}\right)$

Determine $\theta_j = \min(\theta_j^{large}, \theta_{\max})$ where

$$\theta_j^{large} = \frac{1+N}{(j+1)^{1.1}} \min(1, \theta_0, \ldots, \theta_{j-1})$$

$A_{\text{red}} \leftarrow \theta_j \left[l_p\left(\tilde{\boldsymbol{\rho}}^{(j)}\right) - l_p\left(\mathcal{F}_d\left\langle \tilde{\boldsymbol{\rho}}^{(j)} + \mathbf{s}_c \right\rangle\right)\right]$

$P_{\text{red}} \leftarrow -\theta_j \boldsymbol{g}^{\mathrm{T}} \boldsymbol{s}_c$

if $A_{\text{red}} \geq 0.1 P_{\text{red}}$, **then**

$\tilde{\boldsymbol{\rho}}^{(j+1)} \leftarrow \mathcal{F}_d\left\langle \tilde{\boldsymbol{\rho}}^{(j)} + \mathbf{s}_c \right\rangle$

if $A_{\text{red}} \geq 0.5 P_{\text{red}}$, **then**

$\delta_{j+1} \leftarrow \min(2.5\delta_j, ||\boldsymbol{\rho}_u - \boldsymbol{\rho}_l||_\infty)$

else

$\delta_{j+1} \leftarrow \delta_{\min}$

end if

$\theta_{\max} \leftarrow 1$

$\mathbf{g} \leftarrow \partial\mathcal{F}_d\left\langle \nabla l_p(\tilde{\boldsymbol{\rho}}^{(j+1)}) \right\rangle$

$j \leftarrow j + 1$

else

$\delta_j \leftarrow \max(0.25||\mathbf{s}_c||_\infty, 0.1\delta_j)$

$\theta_{\max} \leftarrow \theta_j$

end if

end while

3 Implementation

During the work with the thesis, the theoretical models presented herein have been implemented in computer code in order to be able to consider the numerical examples presented. The implementation have been done in Matlab where scripts and functions have been developed. Some of the Matlab code have also been translated to object oriented Java code.

3.1 Matlab

The Matlab implementation developed consists of a number of functions and scripts that is linked to the formulas and algorithms presented in the theory chapter as well as the optimality criteria method presented in appendix A. The Matlab library is available to download via GitHub[1] and is intended to be compatible with the syntax in the Matlab FE package CALFEM[2].

3.2 Java

One of the initial objectives of this thesis was to create a complete multi-objective topology optimization application in Java that could be run via a web browser. This objective has not been met.

Currently (May, 2013) the application can handle single objective topology optimization with ease using the optimality criteria method. Thanks to an open source Java library for matrix operations called jblas[3], which is based on BLAS and LAPACK libraries, the application solves all evaluated problems faster than Matlab does.

However, the development of the web application had to be postponed for the future due to a number of difficulties that was not possible to overcome within the time limit of the thesis project. One was related to difficulties of finding a suitable equivalent solver for the Matlab `linprog`-solver in Java. Finally, the open source Apache Commons Math SimplexSolver[4] was used. Another issue was the lack of an effective eigenvalue solver in jblas. In the beginning of the thesis project, jblas had an eigenvalue solver that could solve for all eigenvalues of a problem, however only the smallest values are of interest thus the computation time is excessively long using this method. A method for solving for ranges of eigenvalues was developed for jblas within the thesis project and, thanks to the openminded developer of jblas Dr Mikio L. Braun, incorporated into jblas. There was however no time to incorporate this new functionality into the thesis application.

[1] `https://github.com/sehlstrom/motop` – May, 2013
[2] `http://sourceforge.net/projects/calfem/` – May, 2013
[3] `http://jblas.org` – May, 2013
[4] `http://commons.apache.org/proper/commons-math/` – May, 2013

4 Numerical Examples

In this chapter two numerical examples are presented. Firstly, a simply supported beam – a so-called Messerschmitt-Bolkow-Blohm beam – is optimized to withstand a point load at the mid point of the beam; and secondly, the support structure for a long span bridge deck is optimized. In both examples, the Pareto-optimal solutions are tracked for two cases in which different combinations of objectives are considered: 1) volume and compliance and 2) volume, compliance and lowest eigenvalue.

4.1 Messerschmitt-Bolkow-Blohm Beam

The Messerschmitt-Bolkow-Blohm (MBB) beam is commonly used as an example in literature about topology optimization (see e.g. [1, 3, 4, 5, 17]). By the use of multi-objective topology optimization, the task is to find Pareto-optimal structures that can support a point load, $2P = 2$ kN, applied at the mid point of the beam. The distance between the supports is 64 cm and the load is positioned at a height of 20 cm above the support plane. Due to symmetry, only half of the beam is considered, see fig. 4.1.

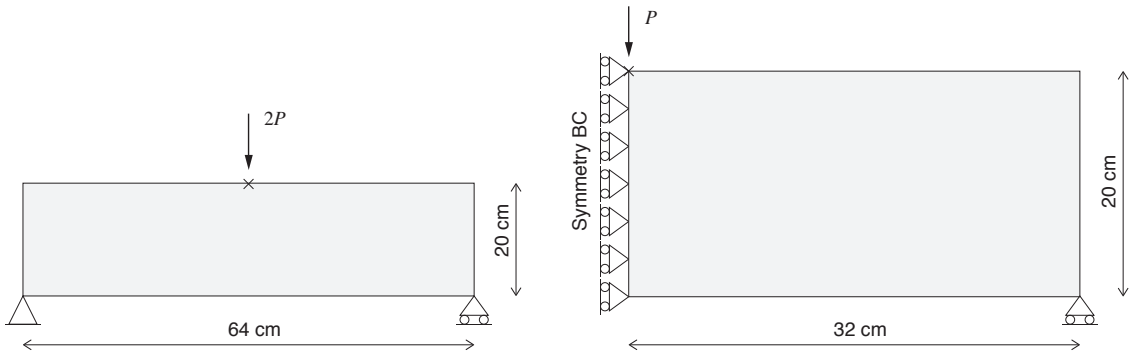

Figure 4.1: *MBB-beam loaded at the midpoint with the point load $2P$. Left: original problem definition. Right: reduced problem definition.*

The beam should be made out of a steel plate of thickness $t = 1.28$ cm (it is assumed that the beam is braced against lateral instability). The steel has the following material parameters: Young's modulus $E^0 = 200$ GPa, Poisson's ratio $\nu^0 = 0.3$ and the density $\rho^0 = 7850$ kg/m^3. The density filter radius is taken as $r_{\min} = 1.28$ cm.

The problem is discretized into the design domain Ω and modeled with square Melosh elements of size 1×1 cm. The Melosh are based on a bilinear displacement approximation and considered to be in plane stress. In order to avoid the trivial eigenvalue solution with infinite eigenvalue when there is no structure, i.e. $\rho_e = 0, \forall e \in \Omega$, some elements are being fixed to be solid: $\rho_e = 1, \forall e \in \Omega^{\text{fixed}}$. The elements that are fixed is the element directly under the load P and the element just above the right hand side support.

In case 1 the ModSIMP interpolation scheme is used with $p = 3$ whereas in

case 2 the RAMP interpolation scheme is used with $q = 20$. Recalling the issue of proper scaling in the objective functions in eq. (2.27); the scaling parameters used are presented in table 4.1 and found using the expressions in eq. (2.28) with $f_{V,\min} = 0.1$.

Table 4.1: Extreme values for volume [m^3], compliance [m/N], and fundamental eigenvalue [-].

Case	$\min V$	$\max V$	$\min C$	$\max C$	$\min \lambda_1$	$\max \lambda_1$
1	8.217e-5	8.192e-4	12e-3	684e-3	-	-
2	8.217e-5	8.192e-4	12e-3	969e-3	2.743e6	3.489e7

4.1.1 Robustness

Next, the robustness in terms of the actual realization of the design where no "gray" structure is allowed is analyzed. The robustness of the optimized designs are quantitatively evaluated by transforming the optimal design $\boldsymbol{\rho}^*$ to a 0-1-design $\boldsymbol{\rho}^{01}$ and then investing the objective difference:

$$\Delta f_i = f_i(\boldsymbol{\rho}^*) - f_i(\boldsymbol{\rho}^{01}), \tag{4.1}$$

where f_i is the objective function considered. The design is considered robust when values of $|\Delta f_i|$ are small.

The transformation between $\boldsymbol{\rho}^*$ and $\boldsymbol{\rho}^{01}$ is done according to:

$$\rho_e^{01} = \begin{cases} 0 & \text{if} \quad \rho_e^* \leq 0.2, \\ 1 & \text{if} \quad \rho_e^* > 0.2, \end{cases} \qquad \forall e \in \Omega, \tag{4.2}$$

where the threshold 0.2 is chosen rather small in order to avoid small islands of material with no connection to the main structure in the 0-1-design. Figure 4.2 shows two examples of how this transformation is working. When evaluating $f_i(\boldsymbol{\rho}^{01})$, only the elements with $\rho_e = 1$ are considered and thus no small stiffnesses $E_{\min}$ or masses $m_{\min}$ are assembled into the stiffness and mass matrices, respectively, in order to avoid singularities; elements that would give rise to these problems are removed completely.

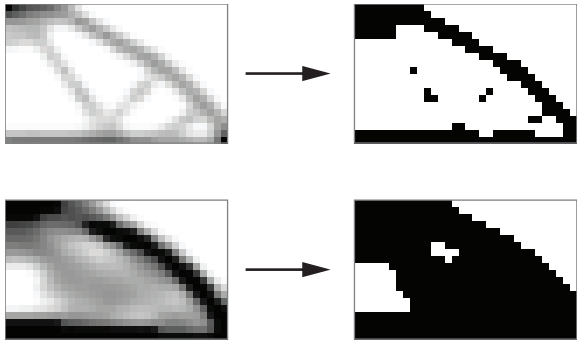

Figure 4.2: *Transformation between* $\boldsymbol{\rho}^*$ *and* $\boldsymbol{\rho}^{01}$.

In order to remove structures that consists of two or more separated – unconnected – substructures when transformed into a 0-1-design we introduce a limit on the

compliance difference; the limit is motivated, from a mathematical point of view, by the fact that the $C(\boldsymbol{\rho}^{01})$ for such a structure will be very large since the stiffness matrix will be singular and, from a physical point of view, such a structure would not provide any support thus failing to transfer applied loads to the supports. The limit is taken as:

$$|\Delta C| \leq 10^9. \tag{4.3}$$

Just as important is the manufacturability of the structure. For this factor, the following limit is introduced:

$$V(\boldsymbol{\rho}^{(k),*}) \geq 0.1 V_\Omega \tag{4.4}$$

4.1.2 Case 1: $\min\left(V(\boldsymbol{\rho}), C(\boldsymbol{\rho})\right)$

The Pareto-optimal solutions are traced using the SLP algorithm along with a continuation method operating on the filter radius which is decreased from a large to a small radius: $r_{\min} = \{5, 4, 3, 2, 1\} \times 0.0128$ cm. For each weight point $k = \{1, 2, \ldots, 21\}$ the compromise weight factors are $w_C^{(k)} = 0.05(21 - k)$ and $w_V^{(k)} = 0.05(k - 1)$ for compliance and for volume, respectively. The initial guess is $\boldsymbol{\rho}^{(1),(0)} = \mathbf{1}$ for $k = 1$ and for the following points $k > 1$ it is taken as $\boldsymbol{\rho}^{(k),(0)} = \boldsymbol{\rho}^{(k-1),*}$.

It should be noted that several other strategies to choose the initial guess where evaluated, both with and without the use of the continuation method. All of these strategies yielded worse result with respect to the compromise value. Most of these strategies also gave structures with larger proportions of gray. Furthermore, mesh dependency have been investigated by reducing the element size to 0.5×0.5 cm and double the number of elements in each direction making the mesh consists of 62×40 elements. No significant difference can be observed when investigating the compromise value and the obtained structures that can motivate the big increase in computation time. It is therefore assumed that the problem is mesh-independent and the coarsest mesh results are considered good enough.

Results

The Pareto-optimal frontier is presented in fig. 4.3 together with some of the obtained structures. All evaluated weight points k but $k = 21$ fulfills the robustness limits of eqs. (4.3) and (4.4). It is, however, expected that the weight point $k = 21$, i.e. where $w_C = 0$, $w_V = 1$ and $\boldsymbol{\rho}^{(21),*} \approx \mathbf{0}$, would not fulfill these limits since the solution obtained is the structure with the lowest possible volume. The result for weight point $k = 1$, i.e. where $w_C = 1$ and $w_V = 0$, is also expected since $\boldsymbol{\rho}^{(1),*} = \mathbf{1}$ yields the stiffest possible structure.

In the same figure, the Pareto-optimal frontier for a single-objective topology optimization is plotted as a dashed line. The single-objective topology optimization is done with the objective to minimize the compliance under a fixed volume fraction constraint: $f_V^{(k)} = V(\boldsymbol{\rho}^{(k),*})/V_\Omega$. As can be seen, the single-objective topology optimization frontier is on or below the multi-objective topology optimization frontier. This implies that the obtained optimal solutions $\boldsymbol{\rho}^{(k),*}$ in fact are not optimal; better results with respect to volume and compliance are possible to find. Performing a check according to eq. (2.32) shows that the norm is in-between 0 and 0.047 for

the different weight points, which is considered small enough to represent a minima point. Together with the single-objective topology optimization results, it can thus be concluded that the obtained solutions are local minima solutions. Furthermore it can be seen that the deviation between the the multi- and single-objective compliance results increases with decreasing volume.

Figure 4.4 shows all obtained Pareto-optimal structures along with the compromise value $l_p\left(\boldsymbol{\rho}^{(k),*}\right)$ and the objective values $V\left(\boldsymbol{\rho}^{(k),*}\right)$ and $C\left(\boldsymbol{\rho}^{(k),*}\right)$. In this figure, it can clearly be seen that, even though distinct structures are forming for most weight points k, the obtained structures are not so-called 0-1-designs. In this example, this is a problem since a variable thickness of the plate is is harder and more costly to manufacture compared to a plate with constant thickness.

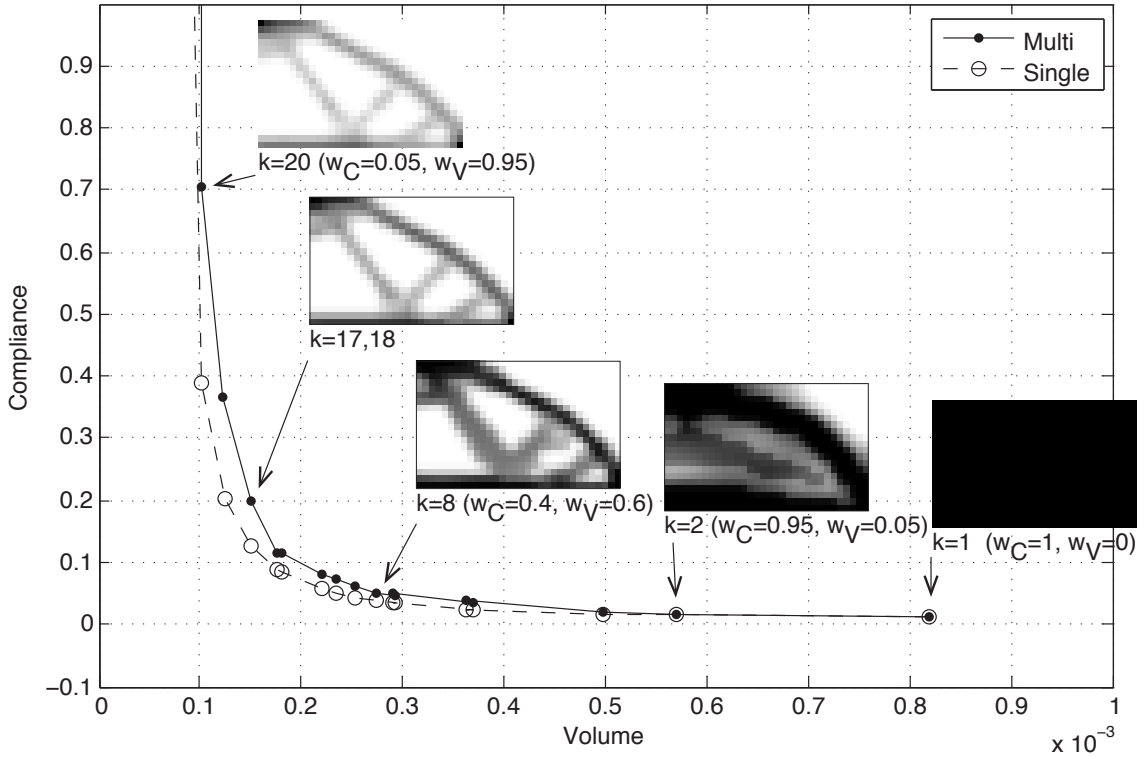

Figure 4.3: *Pareto-optimal frontiers with respect to volume [m^3] and compliance [m/N] with some obtained structures. The solid line is the front obtained when performing multi-objective topology optimization using the SLP algorithm and the dashed line is the front obtained when performing single objective to topology optimization with respect to compliance for a fixed volume fraction.*

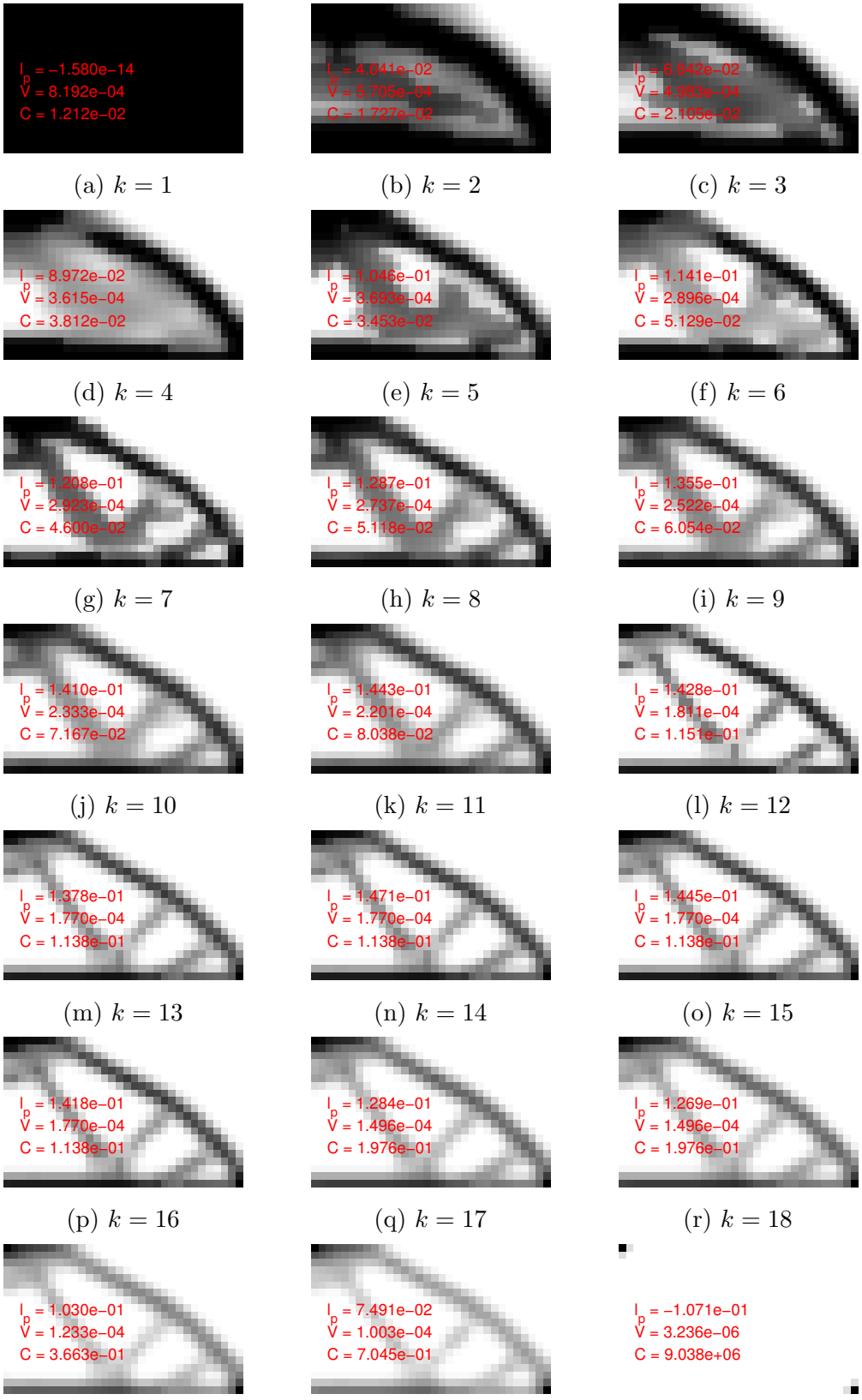

(a) $k = 1$ (b) $k = 2$ (c) $k = 3$

(d) $k = 4$ (e) $k = 5$ (f) $k = 6$

(g) $k = 7$ (h) $k = 8$ (i) $k = 9$

(j) $k = 10$ (k) $k = 11$ (l) $k = 12$

(m) $k = 13$ (n) $k = 14$ (o) $k = 15$

(p) $k = 16$ (q) $k = 17$ (r) $k = 18$

(s) $k = 19$ (t) $k = 20$ (u) $k = 21$

Figure 4.4: *Pareto-optimal structures for each investigated weight point k.*

4.1.3 Case 2: $\min\left(V(\boldsymbol{\rho}), C(\boldsymbol{\rho}), -\lambda_1(\boldsymbol{\rho})\right)$

The Pareto-optimal solutions are investigated using the SLP algorithm along with the continuation method. Just as in case 1, the filter radius is successively decreased: $r_{\min} = \{5, 4, 3, 2, 1\} \times 0.0128$ cm. For each weight point $k = \{1, 2, \ldots, 21\}$ investigated the weights shown in table 4.2 are used. The initial guess is taken as $\boldsymbol{\rho}^{(k),(0)} = \mathbf{1}, \forall k$.

Table 4.2: Points k and their coordinates in weight space.

k	1	2	...	6	7	8	...	11	12	...	20	21
w_V	1	0.80	...	0	0.80	0.60	...	0	0.60	...	0	0
w_{λ_1}	0	0.20	...	1	0	0.20	...	0.80	0	...	0.20	0
w_C	0	0	...	0	0.20	0.20	...	0.20	0.40	...	0.80	1

Just as for case 1, several other strategies to choose the initial guess have been investigated. The one presented here is the strategy that in most cases provided the lowest compromise value. A description of some other strategies evaluated along with the resulting raw data from these strategies can be found in appendix B. The strategy presented here corresponds to "Test 4" in the appendix.

Results

The compromise value $l_p(\boldsymbol{\rho}^*)$ is plotted together with some of the obtained Pareto-optimal structures in fig. 4.5. From this figure it can be seen, just as in case 1, that weight points $k = 1$ and $k = 21$ yields expected results: all voids and all solid, corresponding to $w_V = 1$ and $w_C = 1$, respectively. For the rest of the weight points where the eigenvalue weight factor is zero ($w_{\lambda_1} = 1$), i.e. $k = \{7, 12, 16, 19\}$, the two cases yields different results (c.f. weight points $k = \{17, 13, 9, 5, \}$ in case 1). For the discussed points, case 2 generates bolder structures for points with high weight on the compliance objective whereas for the points with high weight on the volume objective no clear structures are formed at all. There are two possible factors behind these differences. One being the usage of different interpolation schemes in case 1 and 2 and the other being different ways to choose the initial guess.

It can also be seen that the structures obtained when the eigenvalue objective is considered ($w_{\lambda_1} > 0$) are all relatively similar, both in terms of their appearance and in their compromise value. For the structures with higher compromise weight factor, there is a larger portion of gray in the structure than in those with lower compromise weight factor. This can for example be seen when comparing weight points $k = \{8, 9\}$ with weight points $k = \{6, 15\}$.

In fig. 4.6 the objective values are presented together with robustness analysis of each objective. It can be concluded that the volume objective (fig. 4.6a) is almost linearly decreasing with increasing volume weight factor w_V, thus the largest volume is obtained when $w_V = 0$ and the smallest volume is obtained when $w_V = 0$. When it comes to compliance (fig. 4.6c), the weight points $k = \{1, 2, 7\}$ the $|\Delta C|$-value meets the limit of eq. (4.3), see fig. 4.6d. Apart from these points, the compliance is smallest when there is a big volume and highest when the volume is vanishing. Weight

point $k = 4$ do, however, not follow this trend. Here $w_C = 0$, yet the compliance is significantly higher than for the rest of the weight points where $w_C = 0$. This weight point has also the highest eigenvalue, as can be seen in fig. 4.6e.

When looking at the robustness of the three objectives, it becomes evident that the eigenvalue is highly sensitive in comparison to the robustness of the volume and compliance objectives (compare fig. 4.6f with fig. 4.6b and fig. 4.6d).

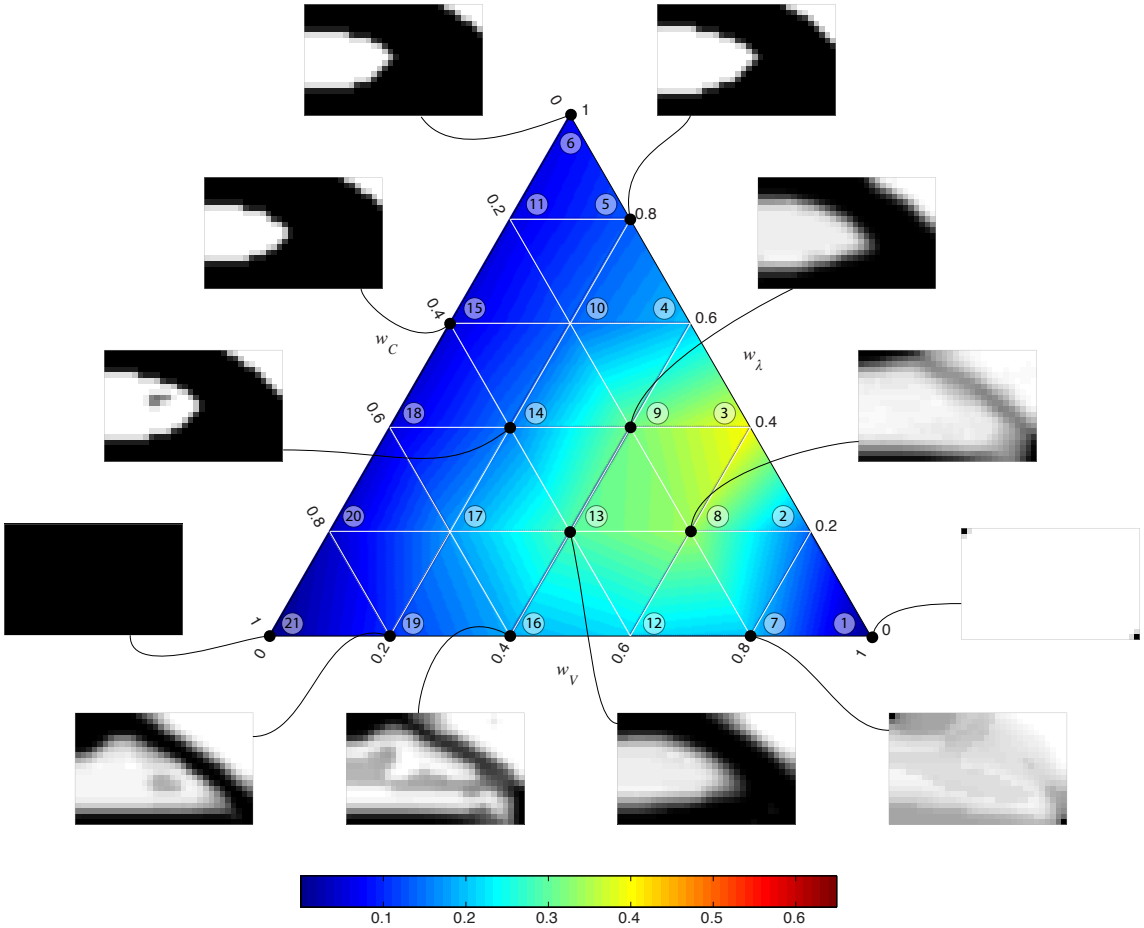

Figure 4.5: *Compromise value $l_p(\boldsymbol{\rho}^*)$ [-] and Pareto-optimal solutions. Weight point numbers k within circles.*

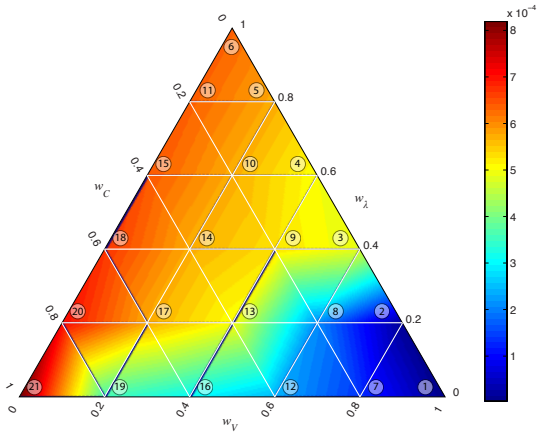

(a) *Volume* $V(\boldsymbol{\rho}^*)$ *[m^3]*

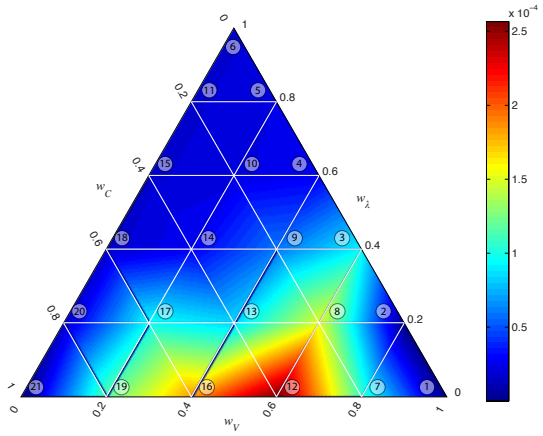

(b) *Volume difference* $|\Delta V|$ *[m^3]*

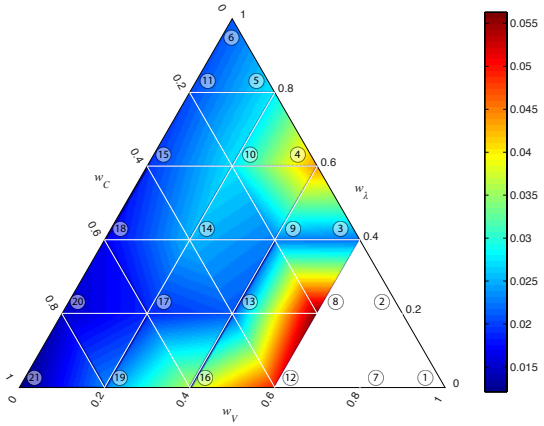

(c) *Compliance* $C(\boldsymbol{\rho}^*)$ *[m/N]*

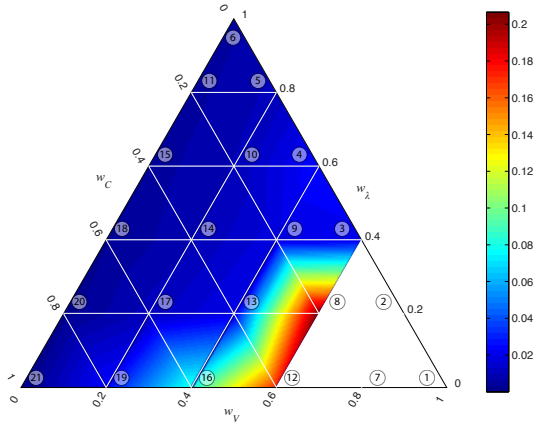

(d) *Compliance difference* $|\Delta C|$*[m/N]*

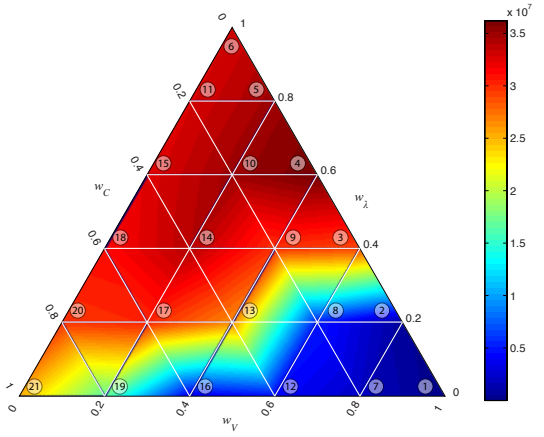

(e) *Eigenvalue* $\lambda_1(\boldsymbol{\rho}^*)$ *[-]*

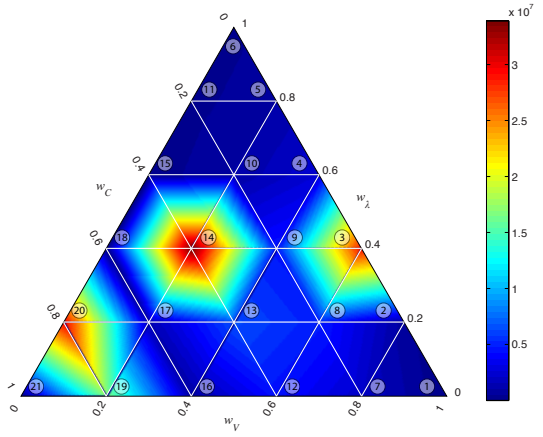

(f) *Eigenvalue difference* $|\Delta\lambda_1|$ *[-]*

Figure 4.6: *Objective results (left) and objective robustness (right). Weight point numbers k within circles.*

4.2 Bridge Design

By the use of multi-objective topology optimization, we here consider the task to investigate conceptual bridge designs across a valley. More precisely, possible designs for the supports of the bridge deck are to be investigated. A schematic overview of the valley and the bridge deck is presented in fig. 4.7. The bridge deck is 74 m long and spans between the points A and B where it is supported on roller bearings. Additional supports may be placed in points C, D, and E and the boat fairway should be clear of any structure to allow for boats passing under the bridge.

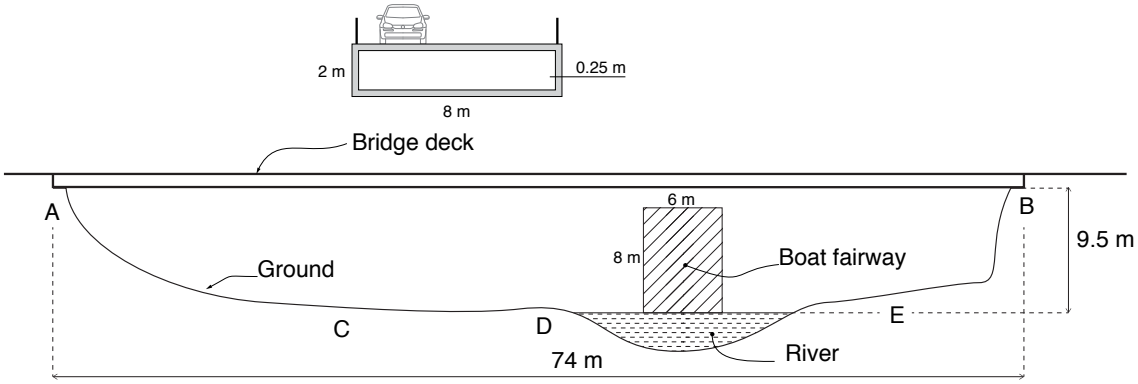

Figure 4.7: *Problem description.*

The bridge supports should be made out of reinforced concrete with a density of $\rho^0 = 2500$ kg/m^3. Young's modulus is taken as $E^0 = 36$ GPa (corresponding to concrete class C45/55, see Table 3.1 in [7]) and it is assumed, in this conceptual investigation, that the concrete is isotropic with a Poisson's ratio of $\nu^0 = 0.2$.

Even though bridges should withstand several hundred of load cases in a true design situation, only one vertical load case, q_d, is taken into consideration representing the self weight of the bridge deck. As indicated in fig. 4.7, the bridge deck made of a rectangular hollow section (RHS) with width 8 m, height 2 m and wall thickness 0.25 m. From this follows that the cross-section area of the deck is $A_d = 4.75$ m^2. The bridge deck is made out of the same concrete as the supports, thus the bridge deck yields a characteristic self load of $q_k = A_d \rho^0 g = 116$ kN/m where g is the gravitational constant. Applying a safety factor of 1.2, the design load is found to be $q_d = 140$ kN/m.

The problem is discretized into the design domain Ω shown in fig. 4.8 and modeled with Melosh elements of size 0.5×0.5 m, thus 148×23 elements are used. The thickness of the design domain is set to 1.2 m and the filter radius is set to $r_{\min} = 0.6$ m implying that the smallest possible support cross-section is about 1.2×1.2 m. The design domain Ω consists of three subdomains: the Ω^{fixed}-subdomain is representing the bridge deck: here $\rho_e = 1$, $\forall e \in \Omega^{\text{fixed}}$; the Ω^{passive}-subdomain is representing the ground and the boat fairway: here $\rho_e = 0$, $\forall e \in \Omega^{\text{passive}}$ – no structure will be placed here; and the Ω^{free} which is the subdomain where the optimized support structure will be placed.

Note that the bridge deck is not modeled accurately here; the bending stiffness of the RHS and the rectangular cross-section obtained using the planar Melosh elements

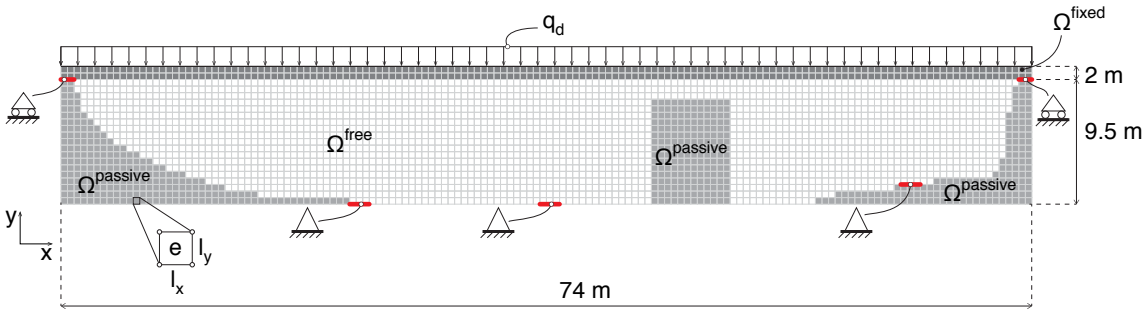

Figure 4.8: *Problem FE-discretization. Note that this figure, due to readability issues, is showing a FE-discretization using elements of size* 1×1 *m, not* 0.5×0.5 *m as in the problem analyzed.*

are not the same. This deviation is twofold: firstly, the bridge deck in the FE-model has a lower bending stiffness than the bending stiffness of the RHS due to the geometry of the sections and secondly, the Melosh element can not model bending action very accurately, even though several layers of elements is used. All together this gives a lower bending stiffness in the model than in the true RHS. This deviation is however neglected in this theoretical example. In a real design situation, the modeling of the bridge deck should be given more care.

In case 1 the ModSIMP interpolation scheme is used with $p = 3$ whereas in case 2 the RAMP interpolation scheme is used with $q = 20$. For each case, the scaling parameters are presented in table 4.3 and found using the expressions in eq. (2.28) with $f_{V,\min} = 0.2$.

Table 4.3: Extreme values for volume [m^3], compliance [m/N], and fundamental eigenvalue [-].

Case	$\min V$	$\max V$	$\min C$	$\max C$	$\min \lambda_1$	$\max \lambda_1$
1	0.208e3	1.021e3	1.250e3	7.362e4	-	-
2	0.208e3	1.021e3	1.250e3	6.720e4	1.921e3	3.682e4

4.2.1 Case 1: $\min\left(V(\boldsymbol{\rho}), C(\boldsymbol{\rho})\right)$

The Pareto-optimal solutions are traced in the same way as in Case 1 for the MBB beam.

Results

The Pareto-optimal frontier is presented in fig. 4.9 together with some of the obtained structures. The result for $w_C = 1$ and for $w_V = 1$ are once again expected. In the figure it can also be seen that several weight points yields the same structure: $k = \{14, 15, 16\}$ and $k = \{18, 19\}$. A single objective topology optimization has been performed for the problem as described in case 1 for the MBB beam. The result is shown in the figure as a dashed line. The single objective optimizaton gives

better results than the multi-objective optimization. A check according to eq. (2.32) confirms together with the single objective optimization results, that the obtained points are local minima points. So far, the results are thus in accordance with the results form case 1 in the MBB example.

In fig. 4.10 all obtained structures are shown along with the compromise and objective values for each weight point k. Here it becomes evident that there is a significant difference between the bridge and the MBB example when it comes to creating clear 0-1-structures. The bridge example yield better 0-1-structures than the MBB example. The likely explanation to this is the presence of some bending stiffness in the bridge deck, thus the optimization can "concentrate" on creating supports that transfers the loading on the bridge deck from some discrete points rather than having to create a widespread support structure that connects to all points along the bridge deck.

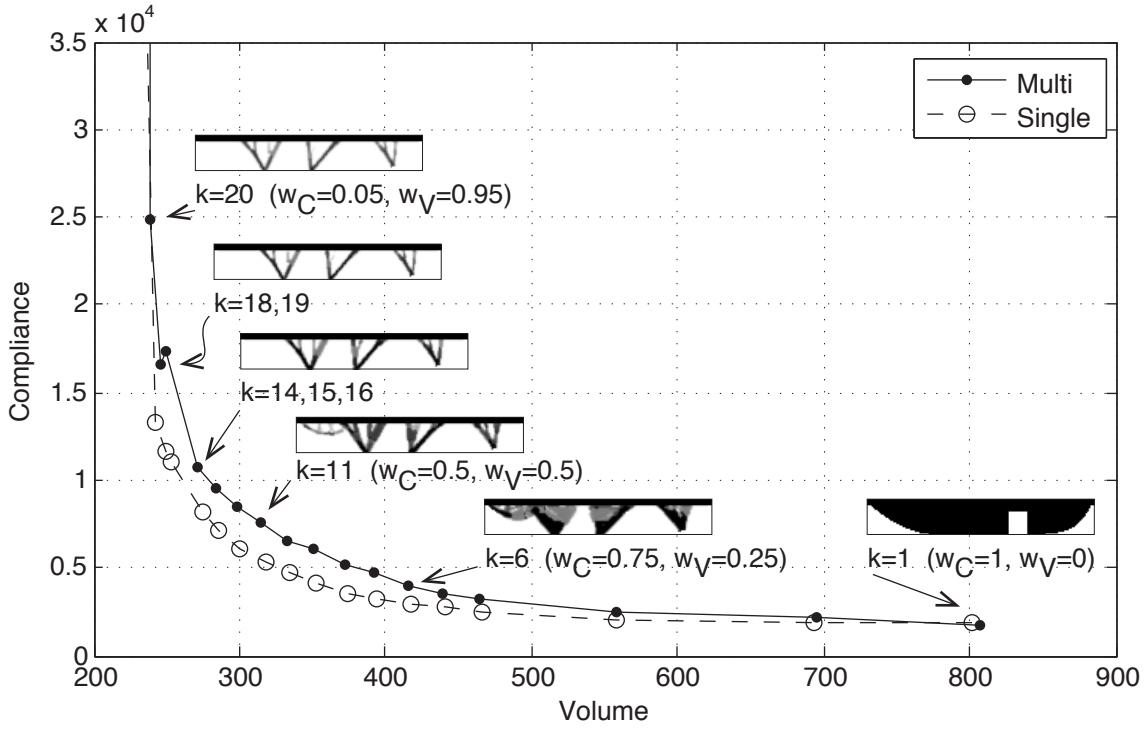

Figure 4.9: *Pareto-optimal frontiers with respect to volume [m^3] and compliance [m/N] with some obtained structures. The solid line is the front obtained when performing multi-objective topology optimization using the SLP algorithm and the dashed line is the front obtained when performing single objective to topology optimization with respect to compliance for a fixed volume fraction.*

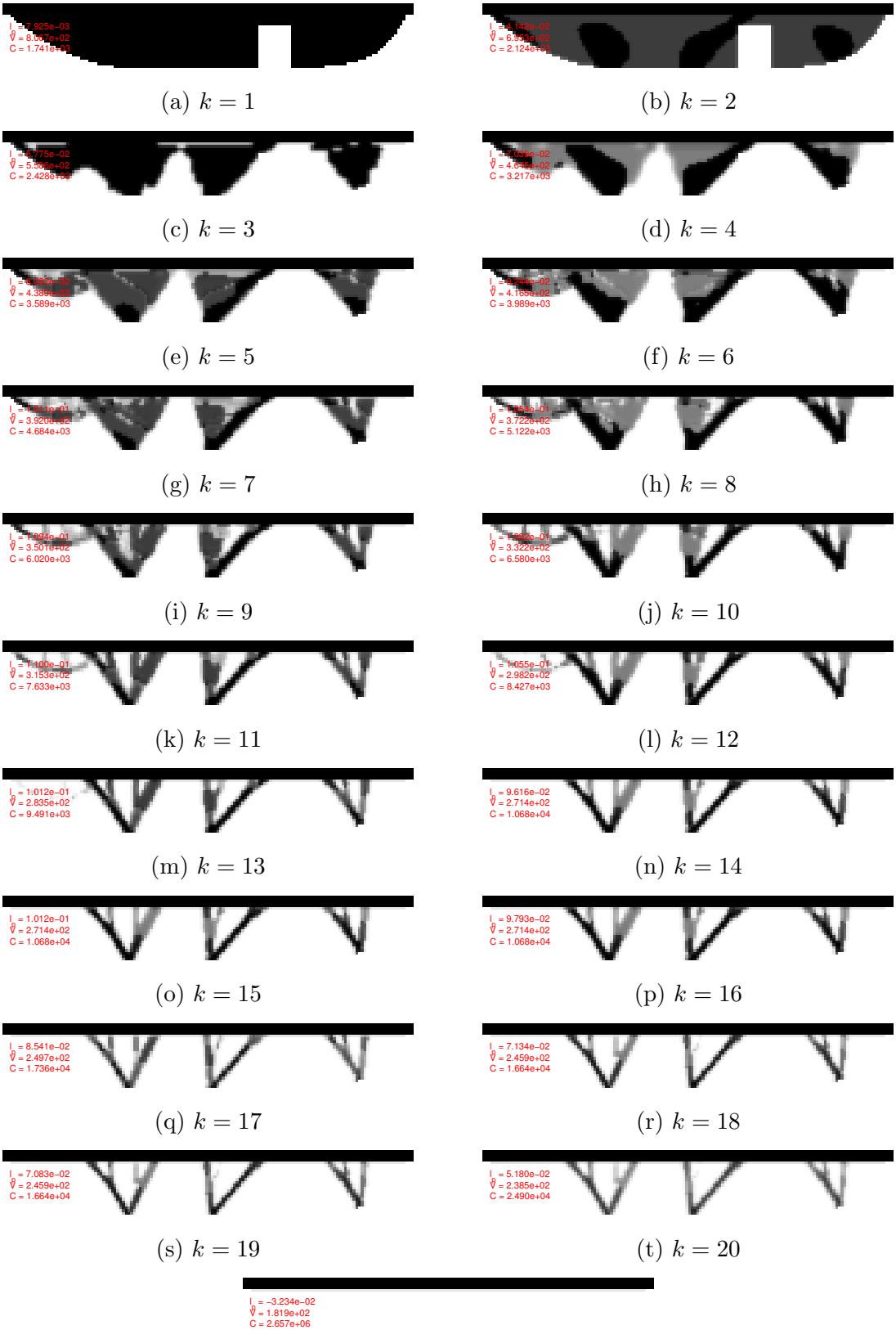

(a) $k = 1$ (b) $k = 2$

(c) $k = 3$ (d) $k = 4$

(e) $k = 5$ (f) $k = 6$

(g) $k = 7$ (h) $k = 8$

(i) $k = 9$ (j) $k = 10$

(k) $k = 11$ (l) $k = 12$

(m) $k = 13$ (n) $k = 14$

(o) $k = 15$ (p) $k = 16$

(q) $k = 17$ (r) $k = 18$

(s) $k = 19$ (t) $k = 20$

(u) $k = 21$

Figure 4.10: *Pareto-optimal structures for each investigated weight point k.*

4.2.2 Case 2: $\min\left(V(\boldsymbol{\rho}), C(\boldsymbol{\rho}), -\lambda_1(\boldsymbol{\rho})\right)$

The Pareto-optimal solutions are traced in the same way as in Case 2 for the MBB beam.

Results

The compromise value $l_p(\boldsymbol{\rho}^*)$ is plotted in fig. 4.11 together with all the obtained Pareto-optimal structures. Here it can be seen that a majority of the weight points gives an optimal structure for $\rho_e = 1 \forall e \in \Omega^{\text{free}}$. These structures make no sense to the problem however since a complete solid structure would not be a bridge at all. For the structures where $w_{\lambda_1} = 0$ bolder structures are formed than in case 1, however there are more "islands" present in case 2. For the rest of the structures, there is no evident trend in the result.

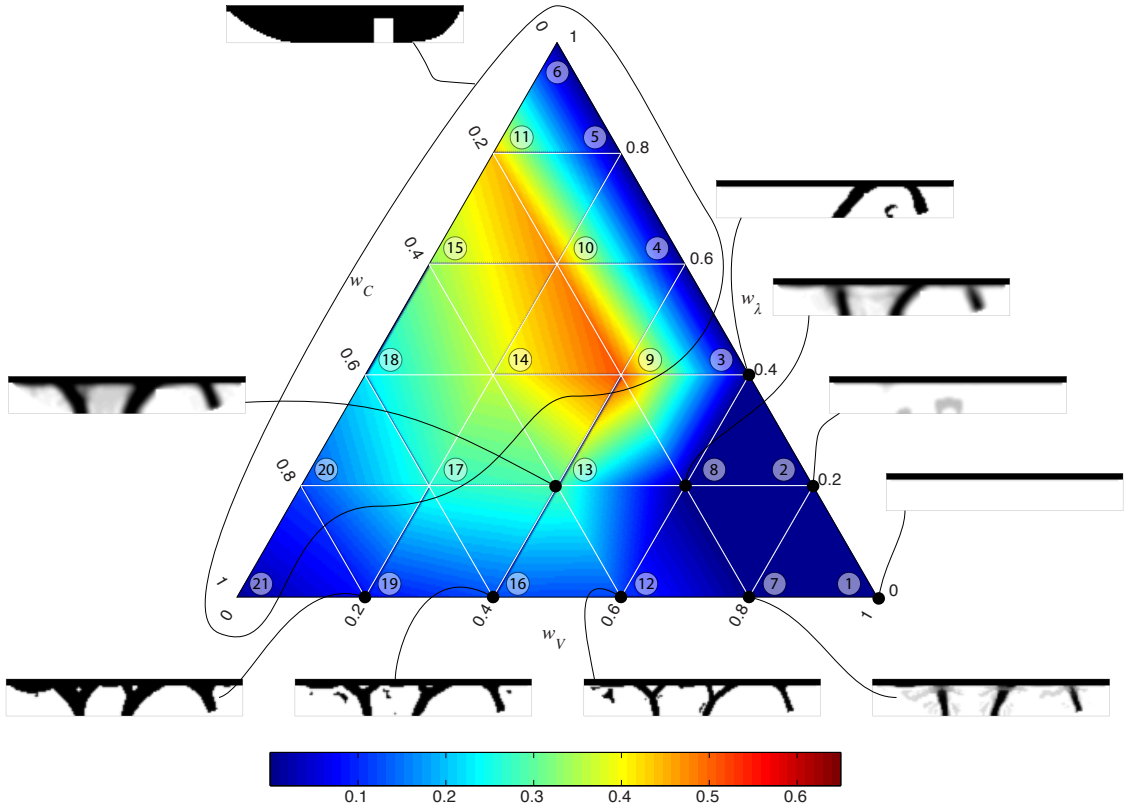

Figure 4.11: *Compromise value $l_p(\boldsymbol{\rho}^*)$ [-] and Pareto-optimal solutions. Weight point numbers k within circles. Note that weight points* 4-6, 9-11, 14-15, 17-18 *and* 20-21 *yields the same result.*

5 Discussion

In this thesis multi-objective topology optimization of structures using Pareto-optimality and a sequential linear programming algorithm has been investigated. More specifically, topology optimization with respect to minimization of weight and compliance, and maximization of the fundamental eigenfrequency has been addressed. The problem formulation is based on the ModSIMP and RAMP interpolations schemes depending on what objectives are considered. Numerical instabilities are reduced using a density filter along with a continuation method on the filter radius.

The common topology optimization problem consisting of a MBB-beam is used as inspiration for the first numerical example presented. In case 1 minimization of compliance and volume is considered and in case 2 the maximization of the lowest eigenvalue is added as well. The MBB example is followed by a bridge design problem for which the same two cases are investigated. The results form the MBB example and the bridge example are in many ways similar, however not as good as one would like them to be. The main issues and their possible causes will be discussed in the following.

5.1 Optimal Solution and Solution Method

In case 1 for both the MBB and the bridge example, it is shown that the obtained Pareto-optimal solutions are in fact not representing global optima points. Furthermore, there seem to be difficulties for the SLP algorithm to find a clear 0-1-structures, a problem not present when performing single objective topology optimization based on the optimality criteria method (recall appendix A). A possible explanation of this might be that the considered objectives are relatively flat around the minima point $\boldsymbol{\rho}^*$, similar to the function $f(x)$ illustrated in fig. 5.1. For such objectives, a large change in the design parameter $\boldsymbol{\rho}$ is needed in order to obtain a small change in the compromise value $l_p(\boldsymbol{\rho})$, however such changes might be hard to perform the way the SLP algorithm is written; the algorithm is decreasing the trust region radius δ_j causing the step length $\mathbf{s}_c$ to decrease until $\boldsymbol{\rho}^{(j)} + \mathbf{s}_c$ is accepted, however if acceptance is never given the algorithm is terminated whiteout finding the minimum point.

5.2 Minimization of Compliance vs. Maximization of Eigenvalue

One can argue that minimizing the compliance and the volume is the same as to maximize the lowest eigenvalue. Since the lowest eigenvalue is found when the stiffness is big and the mass (volume) is low, the argument seems reasonable and is supported by the results from case 2 of the MBB example; the structures where $w_{\lambda_1} > 0$ have a similar appearance to those obtained in case 1. Material is placed at the bottom of the domain and in an arch going from the lower right corner to the upper left corner. But if the results from the bridge example where $w_{\lambda_1} > 0$ is studied, it becomes

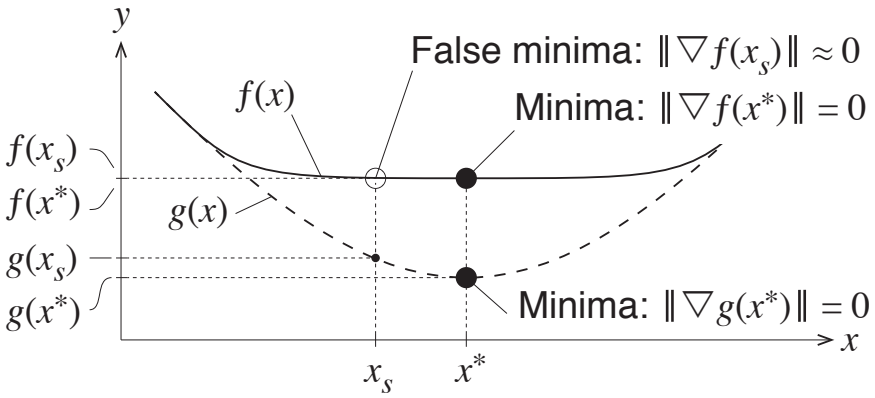

Figure 5.1: *Illustration of two functions $f(x)$ and $g(x)$ with minima points at x^*. The function f is nearly flat around x^* whereas g is convex around x^*. The point $x_s \ll x^*$ is a "false" minima point of f such that $f(x_s) \approx f(x^*)$ and $\|\nabla f(x_s)\| \approx 0$ found after s iteration steps of some optimization algorithm.*

evident that the statement is not true; many of the obtained structures are completely solid, thus has a high stiffness and a large mass.

In fact, to minimize the compliance and volume, and to maximize the lowest eigenvalue will yield different structures in the general case. This is related to compliance being load *dependent* whereas the lowest eigenvalue is load *independent* (recall free vibration limitation). The structure obtained when minimizing the compliance will fit the applied load in the best way, i.e. by applying different loads, different structures will be obtained. The structure obtained when maximizing the lowest eigenvalue will be the same regardless of what load the structure should withstand since the load do not effect the lowest eigenvalue (free vibration).

6 Future Work

Solution Method
In order to clarify whether the issues faced are related to the SLP algorithm used in this thesis, other solution methods should be tested in order to solve the presented problems.

Eigenvalue Scaling
The effect of the scaling parameters for compliance, the $\min C$ and $\max C$ values, have been investigated and some recommendations have been presented based on these investigations. No investigation has however been conducted for the scaling parameters for the eigenvalue. It is likely that these parameters effect the possible findings, just as the compliance scaling parameters. A study of this should be performed in order to ensure reasonable values are used for the scaling of the eigenvalue.

Multiplicity of Eigevalues
The possibility that a structure yields repeated eigenvalues with different mode shapes, e.g. $(\lambda_{1,2}, \boldsymbol{\phi}_1, \boldsymbol{\phi}_2)$, is neglected in the thesis. This is done even though it is very likely that, especially for symmetrical structures, there may occur such eigenvalues; the cost of such considerations have been valued higher than the errors repeating eigenvalues may give. Checks have also been performed when computing the examples presented in the thesis to ensure repeating eigenvalues are not an issue. However, in the case of repeating eigenvalues, the sensitivity analysis formula of the eigenvalue presented herein is no longer valid. This may lead to wrong or poor convergency. In future work, this should be accounted for, e.g. by following the sensitivity analysis presented in [16].

Multiple Load Cases
The optimization can easily be extended to include multiple load cases. This is done by, for each load case c, solving the related displacement $\mathbf{u}^c$ in $\mathbf{K}(\boldsymbol{\rho})\mathbf{u}^c = \mathbf{f}^c$ and then use the obtained displacements to compute the total compliance as:

$$C(\boldsymbol{\rho}) = \sum_{c=1}^{n_c} \left(\sum_{e=1}^{n_{el}} E_e(\boldsymbol{\rho}) (\boldsymbol{u}_e^c)^{\mathrm{T}} \boldsymbol{K}_e^0(\boldsymbol{\rho}) \boldsymbol{u}_e^c \right),$$

where n_c is the number of load cases considered.

3D
Three dimensional design domains should be considered in order to allow for more complex problem setups, e.g. where loads and supports are not in the same plane.

References

[1] E. Andreassen et al. Efficient topology optimization in MATLAB using 88 lines of code. *Structural and Multidisciplinary Optimization* **43** (1 2011), 1–16. ISSN: 1615-147X. DOI: 10.1007/s00158-010-0594-7. URL: http://dx.doi.org/10.1007/s00158-010-0594-7.

[2] M. P. Bendsøe and O. Sigmund. Material interpolation schemes in topology optimization. *Archive of Applied Mechanics* **69** (9-10 1999), 635–654. ISSN: 0939-1533. URL: http://dx.doi.org/10.1007/s004190050248.

[3] M. P. Bendsøe. *Optimization of structural topology, shape, and material*. Lyngby : Danmarks tekniske universitet. Berlin: Springer, 1995. ISBN: 3-540-59057-9.

[4] M. P. Bendsøe and O. Sigmund. *Topology optimization : theory, methods and applications*. 2. ed., corr. pr. Berlin: Springer, 2004.

[5] P. W. Christensen and A. Klarbring. *An introduction to structural optimization*. [Dordrecht]: Springer, 2009. ISBN: 978-1-4020-8665-6.

[6] P. Dombernowsky and A. Søndergaard. "Three-dimensional topology optimisation in architectural and structural design of concrete structures". *Evolution and Trends in Design*. Ed. by D. Alberto and L. Carlos. CMD Domingo y Lázaro Ingenieros SL, 2009, pp. 268 –269. ISBN: 978-84-8363-459-2.

[7] *Eurocode 2 : Design of concrete structures. Part 1-1, General rules and rules for buildings*. 1st ed. Svensk Standard SS-EN 1992-1-1:2005. Stockholm: SIS, 2008.

[8] R. L. Fox and M. P. Kapoor. Rates of change of eigenvalues and eigenvectors. *AIAA Journal* **6**.12 (1968), 2426–2429.

[9] F. A. Gomes and T. A. Senne. An SLP algorithm and its application to topology optimization. *Computational & Applied Mathematics* **30**.1 (2011), 53–89.

[10] J. E. Gordon. *Structures : or Why things don't fall down*. Harmondsworth: Penguin, 1978. ISBN: 0-14-021961-7.

[11] E. Henrysson. Conceptual design and analysis of membrane structures. *Diploma work - Department of Applied Mechanics* 2012:51 (2012). ISSN: 1652-8557. URL: http://publications.lib.chalmers.se/publication/168816-conceptual-design-and-analysis-of-membrane-structures.

[12] *London Olympic Velodrome*. Online. 2011. URL: http://www.isgplc.com/app/article/view.asp?uid=440.

[13] J. Olsson. Form finding and size optimization - Implementation of beam elements and size optimization in real time form finding using dynamic relaxation. *Diploma work - Department of Applied Mechanics* 2012:46 (2012). ISSN: 1652-8557. URL: http://publications.lib.chalmers.se/publication/171108-form-finding-and-size-optimization-implementation-of-beam-elements-and-size-optimization-in-real-tim.

[14] G. Rozvany. Aims, scope, methods, history and unified terminology of computer-aided topology optimization in structural mechanics. *Structural and Multidisciplinary Optimization* **21**.2 (2001), 90–108. ISSN: 1615-147X. URL: http://dx.doi.org/10.1007/s001580050174.

[15] M. Save et al. *Structural optimization. Vol. 2, Mathematical programming*. New York: Plenum, 1990. ISBN: 0-306-41862-2.

[16] A. Seyranian, E. Lund, and N. Olhoff. Multiple eigenvalues in structural optimization problems. *Structural optimization* **8**.4 (1994), 207–227. ISSN: 0934-4373. DOI: 10.1007/BF01742705. URL: http://dx.doi.org/10.1007/BF01742705.

[17] O. Sigmund. A 99 line topology optimization code written in Matlab. *Structural and Multidisciplinary Optimization* **21** (2 2001), 120–127. ISSN: 1615-147X. URL: http://dx.doi.org/10.1007/s001580050176.

[18] O. Sigmund and J. Petersson. Numerical instabilities in topology optimization: A survey on procedures dealing with checkerboards, mesh-dependencies and local minima. *Structural optimization* **16** (1 1998), 68–75. ISSN: 0934-4373. DOI: 10.1007/BF01214002. URL: http://dx.doi.org/10.1007/BF01214002.

[19] O. Sigmund. Morphology-based black and white filters for topology optimization. *Struct Multidisc Optim* **33**.4-5 (2007), 401–424.

[20] O. Sigmund. On the Design of Compliant Mechanisms Using Topology Optimization. *Mechanics of Structures and Machines* **25**.4 (1997), 493–524. DOI: 10.1080/08905459708945415.

[21] M. Stolpe and K. Svanberg. An alternative interpolation scheme for minimum compliance topology optimization. *Structural and Multidisciplinary Optimization* **22**.2 (2001), 116–124. ISSN: 1615-147X. DOI: 10.1007/s001580100129. URL: http://dx.doi.org/10.1007/s001580100129.

[22] unknown. *The Future of Concrete*. Online. 2011. URL: http://www.future-ish.com/2011/08/unikabeton.html.

A Scalar Objective Optimization

In this appendix a single objective topology optimization problem is presented. The objective is to maximize the stiffness of a structure under a volume constraint controlled via a prescribed volume fraction. The ModSIMP interpolation scheme is used along with a sensitivity filter. A solution method suited for the problem is then described.

A.1 Problem Formulation

The problem can be expressed as:

$$\begin{cases} \min\limits_{\boldsymbol{\rho}} & C(\boldsymbol{\rho}) = \mathbf{f}^{\mathrm{T}}\mathbf{u}\{\boldsymbol{\rho}\} \\ \text{subject to} & \begin{cases} \dfrac{V(\boldsymbol{\rho})}{V_\Omega} = f_V \\ \mathbf{K}(\boldsymbol{\rho})\mathbf{u}\{\boldsymbol{\rho}\} = \mathbf{f} \\ \mathbf{0} \leq \boldsymbol{\rho} \leq \mathbf{1} \end{cases} \end{cases}, \tag{A.1}$$

where $C(\boldsymbol{\rho})$ is the objective function representing the compliance of the structure, $\mathbf{u}\{\boldsymbol{\rho}\}$ and $\mathbf{f}$ are the global displacement and force vectors, respectively, $\mathbf{u}_e\{\boldsymbol{\rho}\}$ and $\mathbf{f}_e$ are the element displacement and force vectors, respectively, $\mathbf{K}(\boldsymbol{\rho})$ is the global stiffness matrix, $\boldsymbol{\rho}$ is the vector of design variables representing the generalized density of the mesh, V_Ω is the design domain volume and f_V is the prescribed volume fraction constraint. The total volume of the structure is found from:

$$V(\boldsymbol{\rho}) = \sum_{e=1}^{n_{el}} \rho_e V_e^0, \tag{A.2}$$

where V_e^0 is the base volume of each element and n_{el} is the total number of elements in the mesh. The volume has the derivatives:

$$\frac{\partial V(\boldsymbol{\rho})}{\partial \rho_e} = V_e^0, \qquad \forall e \in \Omega. \tag{A.3}$$

By the use of the equilibrium constraint in eq. (A.1) and the fact that the $\mathbf{K}$-matrix is symmetric, the compliance can be expressed in terms of the stiffness as:

$$C(\boldsymbol{\rho}) = \mathbf{f}^{\mathrm{T}}\mathbf{u}\{\boldsymbol{\rho}\} = \mathbf{u}\{\boldsymbol{\rho}\}^{\mathrm{T}}\mathbf{K}(\boldsymbol{\rho})\mathbf{u}\{\boldsymbol{\rho}\} = \sum_{e=1}^{n_{el}} \boldsymbol{u}_e^{\mathrm{T}} \boldsymbol{K}_e(\rho_e)\boldsymbol{u}_e, \tag{A.4}$$

where $\boldsymbol{u}_e \equiv \boldsymbol{u}_e\{\boldsymbol{\rho}\}$ is the element displacement vector in local coordinates. The element stiffness in local coordinate system is, due to use of the ModSIMP interpolation scheme, found as:

$$\boldsymbol{K}_e(\rho_e) = \left[E_{\min} + \rho_e^p(E_e^0 - E_{\min})\right] \boldsymbol{K}_e^0, \tag{A.5}$$

where $\boldsymbol{K}_e^0$ is the element stiffness matrix in local coordinate system with unit Young's modulus ($E = 1$). Substituting eq. (A.5) into eq. (A.4) gives the compliance:

$$C(\boldsymbol{\rho}) = \sum_{e=1}^{n_{el}} \left[E_{\min} + \rho_e^p (E_e^0 - E_{\min})\right] \boldsymbol{u}_e^{\mathrm{T}} \boldsymbol{K}_e^0 \boldsymbol{u}_e, \tag{A.6}$$

which has the derivatives:

$$\frac{\partial C(\boldsymbol{\rho})}{\partial \rho_e} = -p\rho_e^{p-1}(E_e^0 - E_{\min})\boldsymbol{u}_e^{\mathrm{T}} \boldsymbol{K}_e^0 \boldsymbol{u}_e, \quad \forall e \in \Omega. \tag{A.7}$$

Since the equilibrium constraint in eq. (A.1) was used to find eq. (A.6) we can restate eq. (A.1) as:

$$\begin{cases} \min\limits_{\boldsymbol{\rho}} & C(\boldsymbol{\rho}) = \sum\limits_{e=1}^{n_{el}} \left[E_{\min} + \rho_e^p (E_e^0 - E_{\min})\right] \boldsymbol{u}_e^{\mathrm{T}} \boldsymbol{K}_e^0 \boldsymbol{u}_e \\ \text{subject to} & \begin{cases} \dfrac{V(\boldsymbol{\rho})}{V_\Omega} = f_V \\ \mathbf{0} \leq \boldsymbol{\rho} \leq \mathbf{1} \end{cases} \end{cases} . \tag{A.8}$$

A.2 Optimality Criteria Method (OC)

The optimality criteria (OC) method is an easy and effective way to define an update scheme used iteratively to solve topology optimization problems [3, 4, 5]. OC is applicable on continuous objectives accompanied by one (or several, if generalized [4]) constraints and is based on the method of Lagrangian multipliers. The method defines an update scheme for the design variable and a optimality condition.

Using the ModSIMP interpolation scheme, the update scheme is defined as:

$$\rho_e^{\text{new}} = \begin{cases} \max(0, \rho_e - m) & \text{if} \quad \rho_e (B_e)^\eta \leq \max(0, \rho_e - m) \\ \min(1, \rho_e + m) \leq \rho_e (B_e)^\eta & \text{if} \quad \min(1, \rho_e + m) \leq \rho_e (B_e)^\eta \\ \rho_e (B_e)^\eta & \text{otherwise} \end{cases} , \tag{A.9}$$

and the optimality criteria B_e is defined as:

$$B_e(\lambda) = \frac{-\dfrac{\partial C}{\partial \rho_e}}{\lambda \dfrac{\partial V}{\partial \rho_e}}, \tag{A.10}$$

where λ is a Lagrangian multiplier that can be found using a bi-sectioning algorithm, hence the presence of the positive move limit m (usually $m = 0.2$). Optimality is obtained when $B_e(\lambda) = 1$.

To ensure stability of the update scheme, numerical damping is introduced via η defined as:

$$\eta = \frac{1}{1 + \alpha}, \qquad \alpha > 0. \tag{A.11}$$

A common value for η is 0.5.

The derivations of (A.9) and (A.10) can be found in [4] and further explained in [5].

B MBB Case 2: Alternative Strategies and Results

Four test strategies are presented. The different settings for each strategy are given in table B.1.

In tables B.2 to B.5 the compromise, volume, compliance, and eigenvalue results, respectively, are presented as raw data. The lowest value for each weight point k is marked with green and disqualified results are marked with gray. The tables are followed by four figures, figs. B.1 to B.4, showing the obtained structures for each test, respectively.

Table B.1: Test specific choices.

Test	**Initial guess**	**RAMP parameter**	**Filter radius [m]**
1	$\boldsymbol{\rho}^{(k),(0)} = \mathbf{1}, \forall k$	$q = 20$	$r_{\min} = 0.0128$
2	$\boldsymbol{\rho}^{(k),(0)} = \mathbf{0.5}, \forall k$	$q = 20$	$r_{\min} = 0.0128$
3	$\boldsymbol{\rho}^{(k),(0)} = \mathbf{1}, \forall k$	Continuation method with $q = 0, 1, 2, \ldots, 20$	$r_{\min} = 0.0128$
4	$\boldsymbol{\rho}^{(k),(0)} = \mathbf{1}, \forall k$	$q = 20$	Continuation method with $r_{\min} = [5, 4, 3, 2, 1] \times 0.0128$

Table B.2: Compromise values $l_p(\boldsymbol{\rho}^{(k),*})$ [-] for all test cases at each investigated weight point k. The lowest value for each weight point is marked with green and neglected results marked with gray.

Point k	1	2	3	4	5	6	7
Test 1	-0.1070	0.6239	0.2945	0.2634	0.1980	0.0741	0.2507
Test 2	-0.1070	0.1346	0.3783	0.6082	0.7076	0.3724	0.1846
Test 3	-0.1070	0.1423	0.3721	0.5987	0.6001	0.4046	0.1968
Test 4	-0.1070	0.1396	0.4038	0.2025	0.1338	0.0654	0.2032
Point k	8	9	10	11	12	13	14
Test 1	0.5306	0.2631	0.1874	0.0630	0.2319	0.2500	0.1607
Test 2	0.3510	0.5589	0.4643	0.1674	0.2440	0.3262	0.3497
Test 3	0.3753	0.4661	0.2905	0.2550	0.1997	0.3051	0.2259
Test 4	0.3423	0.3152	0.1393	0.0572	0.2191	0.2928	0.1537
Point k	15	16	17	18	19	20	21
Test 1	0.0522	0.1974	0.1559	0.0604	0.1424	0.0368	0.0000
Test 2	0.0861	0.1843	0.3203	0.0604	0.1646	0.0368	0.0000
Test 3	0.1636	0.1644	0.2490	0.1373	0.1137	0.0767	0.0000
Test 4	0.0510	0.1871	0.1742	0.0515	0.1049	0.0376	0.0000

Table B.3: Volume $V(\boldsymbol{\rho}^{(k),*})$ [m^3] for all test cases at each investigated weight point k. The lowest value for each weight point is marked with green and neglected results marked with gray.

Point k	1	2	3	4	5	6	7
Test 1	3.24e-6	5.07e-4	4.57e-4	5.66e-4	6.23e-4	6.41e-4	2.31e-4
Test 2	3.24e-6	5.59e-6	1.31e-5	6.72e-5	2.70e-4	5.91e-4	1.36e-4
Test 3	3.24e-6	1.96e-5	4.25e-5	1.81e-4	3.49e-4	5.48e-4	1.26e-4
Test 4	3.24e-6	1.51e-5	4.85e-4	5.01e-4	5.70e-4	6.31e-4	1.40e-4
Point k	8	9	10	11	12	13	14
Test 1	6.10e-4	5.54e-4	6.18e-4	6.43e-4	2.06e-4	5.13e-4	5.95e-4
Test 2	1.61e-4	1.81e-4	5.39e-4	6.64e-4	1.91e-4	2.97e-4	5.60e-4
Test 3	1.69e-4	2.27e-4	4.54e-4	5.07e-4	1.99e-4	2.58e-4	4.18e-4
Test 4	2.11e-4	5.28e-4	5.70e-4	6.34e-4	2.43e-4	5.02e-4	5.69e-4
Point k	15	16	17	18	19	20	21
Test 1	6.45e-4	3.03e-4	5.89e-4	6.87e-4	3.94e-4	7.04e-4	8.19e-4
Test 2	6.80e-4	2.98e-4	5.34e-4	6.87e-4	6.80e-4	7.04e-4	8.19e-4
Test 3	5.11e-4	2.52e-4	5.57e-4	4.90e-4	3.75e-4	5.11e-4	8.19e-4
Test 4	6.41e-4	3.04e-4	5.71e-4	6.68e-4	3.56e-4	7.04e-4	8.19e-4

Table B.4: Compliance $C(\boldsymbol{\rho}^{(k),*})$ [m/N] for all test cases at each investigated weight point k. The lowest value for each weight point is marked with green and neglected results marked with gray.

Point k	1	2	3	4	5	6	7
Test 1	8.84e+6	6.81e-2	8.24e-2	3.81e-2	2.67e-2	2.51e-2	4.38e-1
Test 2	8.84e+6	8.56e+6	8.04e+6	2.49e+0	3.63e-1	3.12e-2	6.15e-1
Test 3	8.84e+6	1.55e+1	5.40e+0	6.66e-1	2.51e-1	1.25e-1	7.24e-1
Test 4	8.84e+6	2.03e+1	4.38e-2	6.99e-2	3.85e-2	2.67e-2	6.82e-1
Point k	8	9	10	11	12	13	14
Test 1	3.17e-2	3.84e-2	2.58e-2	2.44e-2	3.23e-1	3.97e-2	2.78e-2
Test 2	4.44e-1	5.02e-1	4.62e-2	2.17e-2	3.82e-1	1.29e-1	3.27e-2
Test 3	5.15e-1	2.71e-1	9.23e-2	1.25e-1	2.61e-1	1.48e-1	9.23e-2
Test 4	2.63e-1	4.13e-2	3.73e-2	2.57e-2	2.23e-1	4.14e-2	3.44e-2
Point k	15	16	17	18	19	20	21
Test 1	2.36e-2	1.35e-1	2.57e-2	1.84e-2	8.09e-2	1.63e-2	1.21e-2
Test 2	1.86e-2	1.19e-1	4.56e-2	1.84e-2	1.50e-2	1.63e-2	1.21e-2
Test 3	7.10e-2	1.27e-1	3.79e-2	7.45e-2	5.30e-2	4.81e-2	1.21e-2
Test 4	2.41e-2	1.18e-1	3.01e-2	1.97e-2	4.86e-2	1.67e-2	1.21e-2

Table B.5: eigenvalues $\lambda_1(\boldsymbol{\rho}^{(k),*})$ [-] for all test cases at each investigated weight point k. The highest value for weight point point is marked with green and neglected results marked with gray.

Point k	1	2	3	4	5	6	7
Test 1	7.70e+0	8.77e+6	3.57e+7	3.48e+7	3.28e+7	3.25e+7	2.17e+6
Test 2	7.70e+0	6.81e+0	4.74e+0	1.89e+6	8.52e+6	2.29e+7	2.66e+6
Test 3	7.70e+0	1.19e+6	2.41e+6	6.15e+6	1.37e+7	2.54e+7	2.51e+6
Test 4	7.70e+0	7.77e+5	2.88e+7	3.62e+7	3.48e+7	3.28e+7	2.22e+6
Point k	8	9	10	11	12	13	14
Test 1	1.93e+7	3.48e+7	3.28e+7	3.25e+7	3.46e+6	3.42e+7	3.37e+7
Test 2	3.39e+6	2.59e+6	1.70e+7	2.88e+7	3.15e+6	9.09e+6	1.79e+7
Test 3	2.88e+6	8.12e+6	2.56e+7	2.56e+7	4.90e+6	1.04e+7	2.68e+7
Test 4	5.15e+6	2.95e+7	3.48e+7	3.27e+7	4.47e+6	2.64e+7	3.39e+7
Point k	15	16	17	18	19	20	21
Test 1	3.23e+7	6.84e+6	3.33e+7	3.04e+7	8.57e+6	2.95e+7	2.49e+7
Test 2	3.04e+7	7.42e+6	6.50e+6	3.04e+7	2.16e+7	2.95e+7	2.49e+7
Test 3	3.11e+7	8.39e+6	1.82e+7	3.09e+7	1.45e+7	3.06e+7	2.49e+7
Test 4	3.24e+7	3.35e+6	3.00e+7	3.11e+7	1.67e+7	2.95e+7	2.49e+7

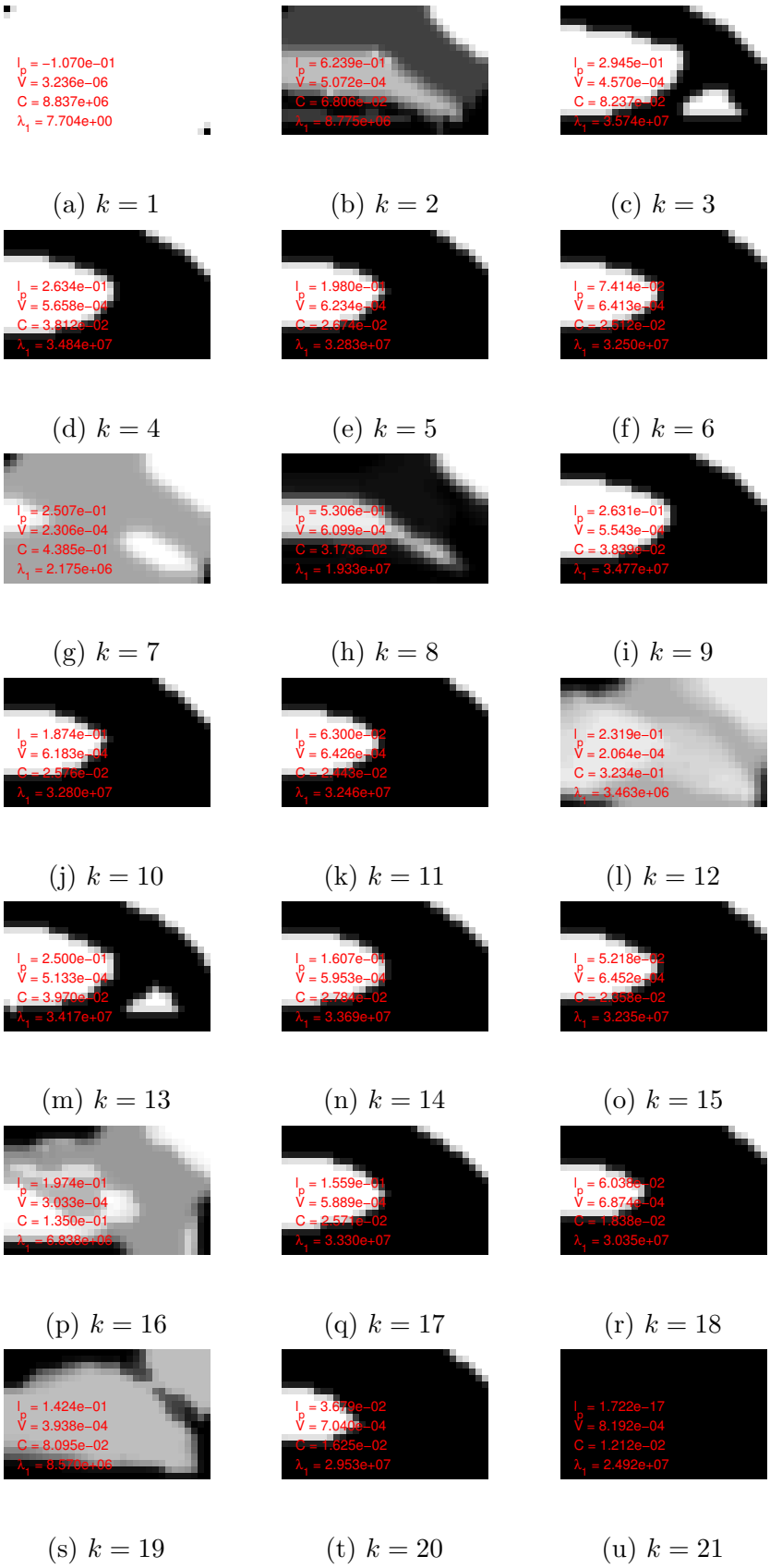

(a) $k = 1$ (b) $k = 2$ (c) $k = 3$

(d) $k = 4$ (e) $k = 5$ (f) $k = 6$

(g) $k = 7$ (h) $k = 8$ (i) $k = 9$

(j) $k = 10$ (k) $k = 11$ (l) $k = 12$

(m) $k = 13$ (n) $k = 14$ (o) $k = 15$

(p) $k = 16$ (q) $k = 17$ (r) $k = 18$

(s) $k = 19$ (t) $k = 20$ (u) $k = 21$

Figure B.1: *Test 1: Pareto-optimal structures for each weight point k.*

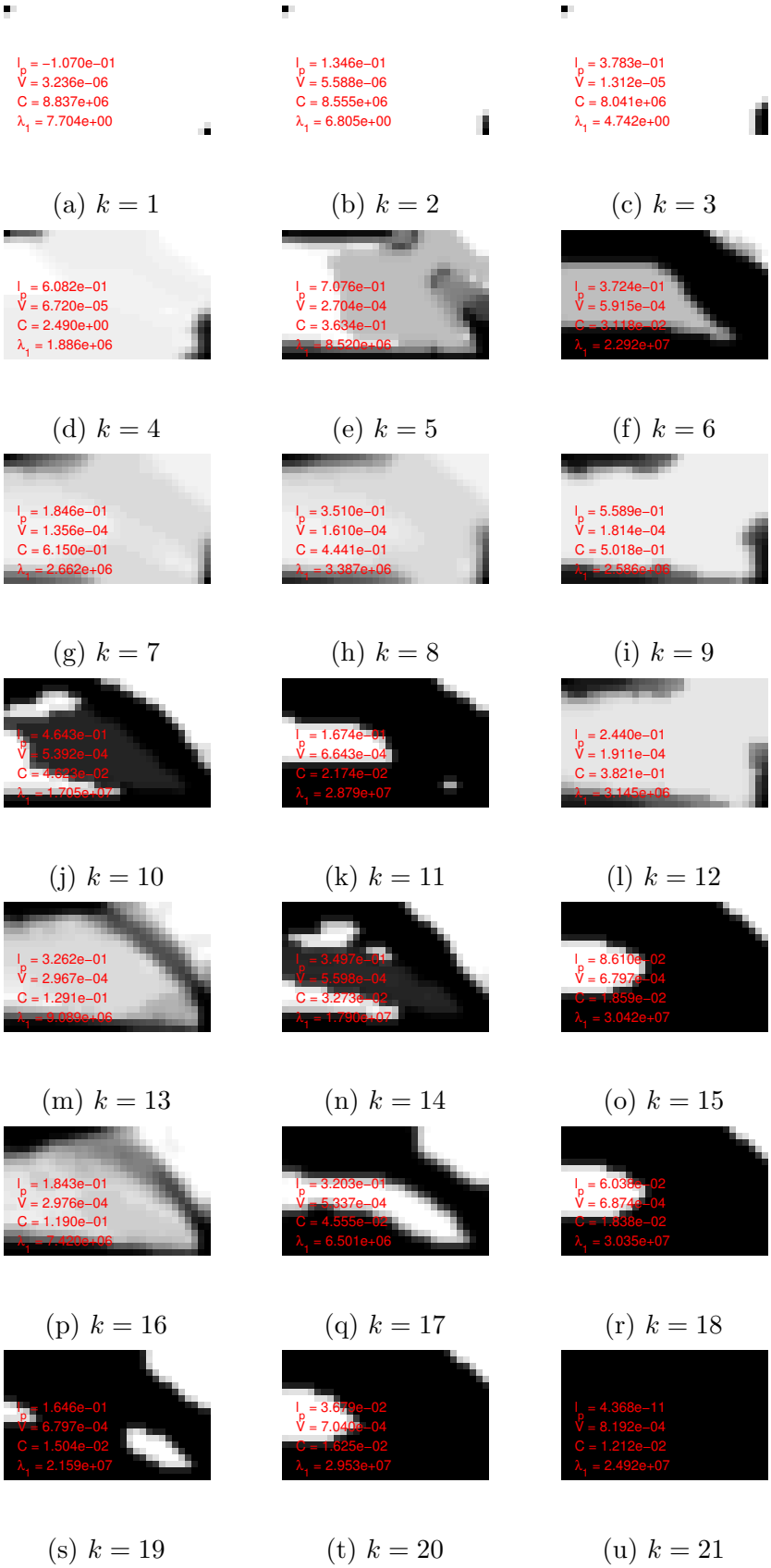

Figure B.2: *Test 2: Pareto-optimal structures for each weight point k.*

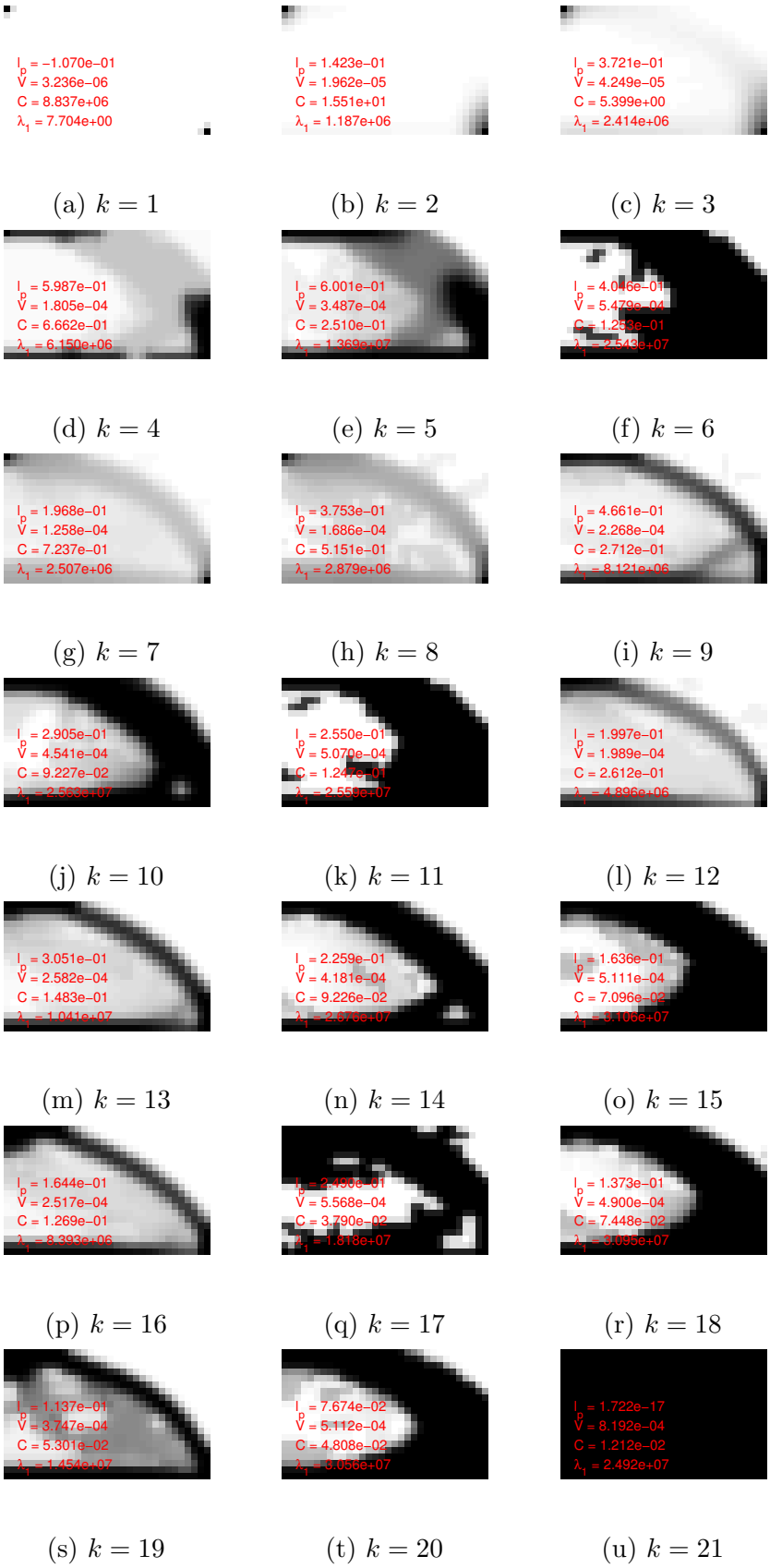

Figure B.3: *Test 3: Pareto-optimal structures for each weight point k.*

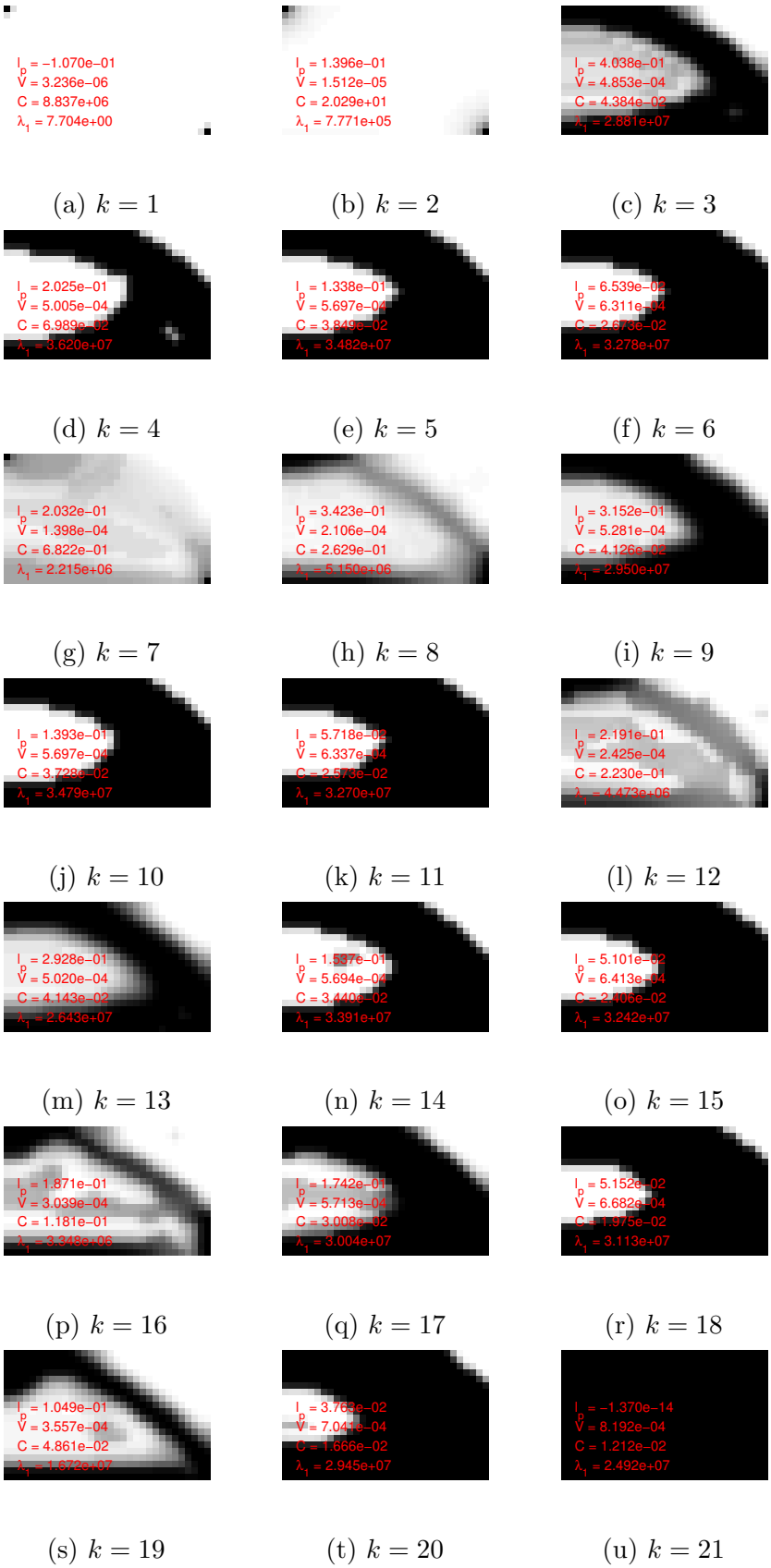

(a) $k = 1$ (b) $k = 2$ (c) $k = 3$

(d) $k = 4$ (e) $k = 5$ (f) $k = 6$

(g) $k = 7$ (h) $k = 8$ (i) $k = 9$

(j) $k = 10$ (k) $k = 11$ (l) $k = 12$

(m) $k = 13$ (n) $k = 14$ (o) $k = 15$

(p) $k = 16$ (q) $k = 17$ (r) $k = 18$

(s) $k = 19$ (t) $k = 20$ (u) $k = 21$

Figure B.4: *Test 4: Pareto-optimal structures for each weight point k.*